How important is reactor design for CO_2 conversion in warm plasmas?

Rani Vertongen [*], Annemie Bogaerts [*]

Research group PLASMANT, Department of Chemistry, University of Antwerp, Belgium

ARTICLE INFO

ABSTRACT

In this work, we evaluated several new electrode configurations for CO_2 conversion in a gliding arc plasmatron (GAP) reactor. Although the reactor design influences the performance, the best results give only slightly higher CO_2 conversion than the basic GAP reactor design, which indicates that this reactor may have reached its performance limits. Moreover, we compared our results to those of four completely different plasma reactors, also operating at atmospheric pressure and with contact between the plasma and the electrodes. Surprisingly, the performance of all these warm plasmas is very similar (CO_2 conversion around 10 % for an energy efficiency around 30 %). In view of these apparent performance limits regarding the reactor design, we believe further improvements should focus on other aspects, such as the post-plasma-region where the implementation of nozzles or a carbon bed are promising. We summarize the performance of our GAP reactor by comparing the energy efficiency and CO_2 conversion for all different plasma reactors reported in literature. We can conclude that the GAP is not the best plasma reactor, but its operation at atmospheric pressure makes it appealing for industrial application. We believe that future efforts should focus on process design, techno-economic assessments and large-scale demonstrations: these will be crucial to assess the real industrial potential of this warm plasma technology.

1. Introduction

The current linear carbon economy leads to increasing CO_2 emissions and we need urgent action for the transition to a more sustainable society [1]. The implementation of renewable electricity is the crucial first step in reducing the CO_2 emissions [2], but industrial electrification brings new challenges. Since carbon products will not disappear entirely, careful management of the CO_2 that is already in the atmosphere and recycling human CO_2 emissions will be key to minimizing the environmental risks [3]. Carbon capture and storage (CCS) is the most promising group of technologies that can effectively decrease the CO_2 emissions before 2050 [4], but large-scale implementation is only just starting [5–7]. Therefore, a complementary mitigation pathway is to utilize this captured CO_2 as a feedstock for cleaner processes (carbon capture and utilization, CCU) [8]. In this context, several technologies are being developed for CO_2 conversion, including plasma technology [9].

Plasma technology has been demonstrated in various industrial applications, such as ozone production and arc plasma furnaces for steelmaking [10]. In recent decades, it is gaining increasing attention for the conversion of stable molecules, like N_2 for fertilizer production

(nitrogen fixation) [11–14] or CO_2 conversion into value-added chemicals [15]. Plasma is an ionized gas that activates these stable molecules at ambient conditions. Other advantages include the instant control of the process (making it ideal to combine with fluctuating renewable electricity), the overall flexibility of input gases and the fact that it does not require scarce materials. [15].

Various types of plasma reactors have already been examined for CO_2 conversion [15] and the gliding arc plasmatron (GAP) is one of the most promising configurations [16,17]. For pure CO_2 splitting, the GAP reactor achieved energy efficiencies up to 30 %, although the conversion remained limited to a maximum of 8.6 % [17]. Other processes, using different gas mixtures, such as dry reforming of methane [18,19] and nitrogen fixation [20,21] show promising results as well. In order to become a competitive technology [15] and address the scale needed for climate change mitigation [4], further improvements are needed.

A lot of research has been performed regarding the improvement of plasma reactor design. Many examples in literature show that small changes in the geometry can have a significant impact on the results. Lu et al. [22] investigated the internal angle in a rotating gliding arc (RGA) reactor, which proved to be an important parameter for the stability of dry reforming of methane. An angle of 45° was clearly more favourable,

increasing the energy efficiency by 25 % when compared to angles of 30° and 60°. Guofeng et al. [23] studied a design very similar to the GAP for partial oxidation of methane. When they increased the reactor length from 5 to 15 mm, the energy efficiency increased about 10 %. They attributed this improvement to the longer residence time of the gas in the plasma, although the input power was insufficient to sustain even longer plasmas. They also studied the ratio of the outlet diameter to the inner diameter and the performance was optimal at a 0.5 ratio, which is comparable to the findings of Ramakers et al. [17] for the GAP design. A more innovative electrode design was invented by Trenchev et al. [24]: the dual vortex plasmatron (DVP). Here, the arc elongates in two directions to increase the residence time of the gas inside the plasma, and by strong rotation of the arc, the gas convection actively cools the cathode spot. The conversion was again around 9 %, for a higher energy efficiency of 41 %, but the limited power supply unit was an obstacle for exploiting the design's full potential. Further performance enhancements might be possible at higher power. Another combined modelling and experimental study by Trenchev et al. [25] revealed significant optimisations for an atmospheric pressure glow discharge (APGD). The best results were obtained with the so-called confined APGD. In this set-up, a ceramic tube is inserted closely around the cathode pin, to increase the gas fraction passing through the plasma and enable wall stabilisation. Thanks to the groove in the cathode pin, the electrode is cooled effectively, which allows for higher powers at lower flow rates. As a result, the design allows a higher specific energy input and improves the stability of the plasma, which explains the enhanced performance: the conversion increased to 12.5 %, as opposed to 4.5 % in the basic pin-to-plate design. A small disadvantage was that more heat and plasma species are lost on the walls, which slightly reduced the energy efficiency. Similar studies can be found for other improvements of plasma reactors, such as the reactor structure of a DBD [26,27], magnetic stabilisation in GA reactors [28–30], confining the gas in the plasma [31], the implementation of nozzles [32–37] and alternative flow patterns [38,39].

Smart reactor design seems essential to enhance the performance of gas conversion. In case of the GAP reactor, the design was previously investigated by Trenchev et al. [40] with a combined modelling approach of 3D fluid dynamics and 2D plasma chemistry. Although the characteristic reverse vortex flow (RVF) is beneficial to stabilise the discharge in the centre of the reactor, it was suggested that not all the gas passes through the discharge zone. A significant amount of gas seems to leave the reactor without being in touch with the plasma. Their

findings confirmed the experimental observations of Ramakers et al. [17] who found that a smaller outlet diameter of 7.08 mm yielded a much higher CO_2 conversion of 8.6 % compared to 6 % and 5 % for the larger outlet diameters of 14.2 mm and 17.5 mm, respectively. They attributed this improved performance to the more pronounced RVF in the design with the smallest outlet diameter and argued that this forces a higher residence time of the gas in the plasma. This stronger RVF also provides thermal insulation of the discharge from the walls, which reduces the thermal losses. In addition, the reactor with the smallest outlet diameter displayed the longest afterglow. Such a larger active plasma volume could also explain the improved performance. Varying the outlet diameter yielded promising results, but so far, no further reactor design improvements were investigated.

In this work, we explored several new variations in electrode shapes within the existing GAP reactor, to investigate the influence on the CO_2 conversion and energy efficiency. Furthermore, we compare our results to the performance of plasma reactors with a completely different design, to gain a deeper understanding of possible improvements. Finally, we put our experimental results in context of the state-of-the-art and propose routes for further optimisation.

The paper is structured as follows. First, we describe the general experimental set-up and reactor designs in Section 2. The experimental results of the different electrode designs are described in Section 3. We summarise the results of all designs in Section 4 and discuss them in Section 5 compared to all recent literature on plasma-based CO_2 conversion. Finally, the overall conclusion is presented in Section 6.

2. Methods

2.1. Experimental setup

The experimental setup is shown in Fig. 1 and is similar to the setup described by Ramakers et al. [17]. A mass flow controller (Bronkhorst El-Flow Select type F-201AV-50 K) was used to insert CO_2 into the reactor, with a purity of 99.5 % and without preheating the gas. The flow rate was varied between 10 and 20 L_s min^{-1}. The reactor was powered by a custom-built DC current source type power supply. The voltage signal was measured with a high voltage probe with a 1:1000 ratio (Cal Test Electronics CT4028) while the current signal was acquired using a 2 Ω shunt resistor. The electric signals were sampled with a two-channel digital storage oscilloscope (Keysight DSO-X 1102 A 100 MHz). The plasma power was calculated from the product of the measured voltage
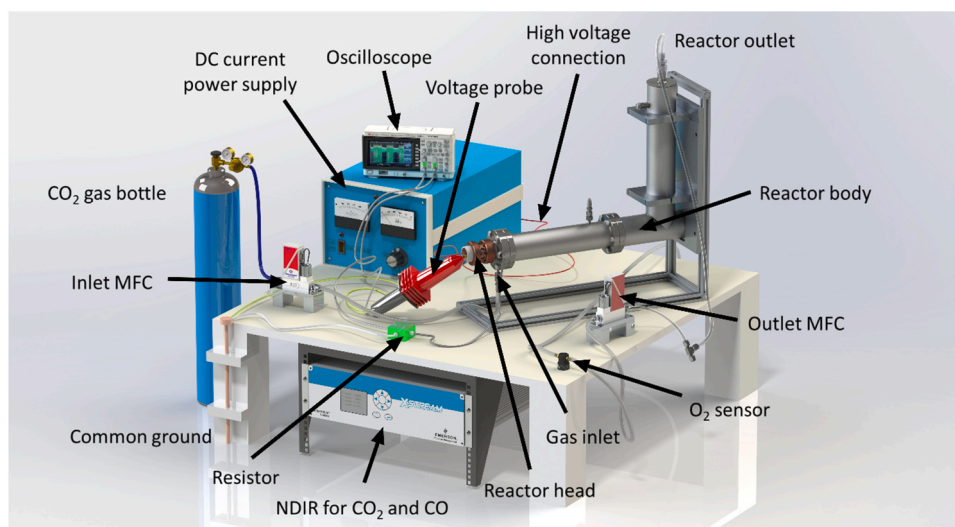

Fig. 1. Experimental setup used for CO_2 splitting. The reactor head is explained in more detail in Fig. 2 and previous work [41]. The reactor body has an L-shape in order to diminish the vortex flow before arriving at the diagnostics. The Faraday cage is not displayed to show each component more clearly. A 2D scheme is provided in the Supporting Information (SI, section S1) with a better view on the connection of all components.
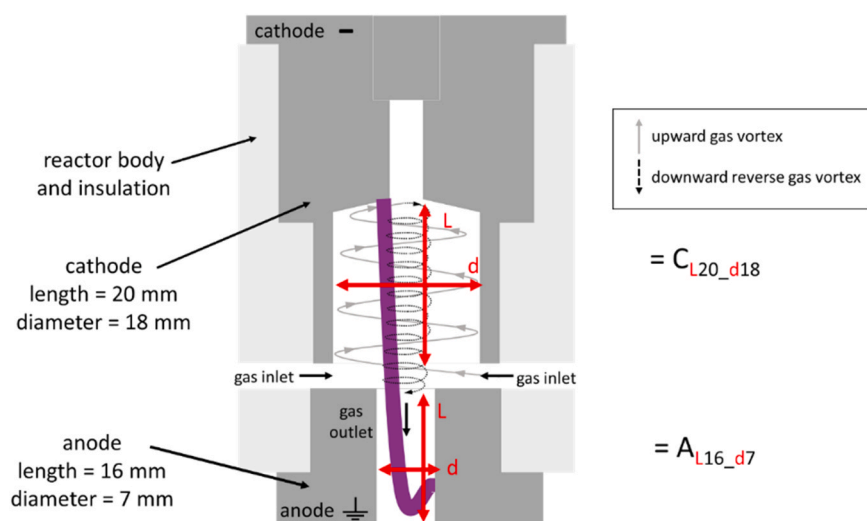
Fig. 2. Schematic 2D representation of the basic GAP reactor. Dark grey indicates the cathode and anode electrodes, light grey represents how they fit into the reactor body. The white space represents the gas volume. The upand downward vortex of the gas are schematically represented in grey and black, respectively, and an artistic presentation of the arc is presented in purple. The gas flows in through six tangential inlets from the side, goes inside the reactor volume and then flows out through the anode. The dimensions are indicated by red arrows (d = diameter and L = length) which is included in the name of each electrode (indicated on the right of the figure: C_{L20_d18} and A_{L16_d7}). The top of the cathode contains an axial inlet that is closed off, but the hole above the main cathode body helps to prevent electrode damage since the arc does not attach in a single point.

and the current. After the reactor, the outlet gas was sampled with a mass flow controller (Bronkhorst type F-200DV Low dP) and sent to an online NDIR (Non-Dispersive Infrared Spectroscopy, Emerson XEPG) and an optical oxygen sensor (Pyroscience). The reactor and power supply were placed inside a Faraday cage.

In this work, we focus on the performance for gas conversion by measuring the outlet gas mixture and the plasma power. Since the reactor is made from stainless steel, no optical in-situ measurements are possible and detailed plasma characterization is beyond the scope of this work. For more information, we refer the reader to earlier work in the GAP [40–42] and in similar reactor geometries [43].

2.2. Reactor design

The inside of the basic design of the GAP reactor is explained in more detail in Fig. 2.

Fig. 2 illustrates the concept of this GAP, using a reverse vortex flow (RVF). The gas flows into the reactor through tangential inlets, and an arc forms between both electrodes (purple). First, the cold gas from the inlets flows upwards close to the walls (outer spiral) creating an isolating and cooling effect. Afterwards, it flows downwards in a reverse vortex (inner spiral) where it mixes with the plasma. Ramakers et al. [17] demonstrated a large improvement by varying the anode diameter. They observed that with larger anode diameters (14–17 mm), a larger fraction of the gas flows directly to the outlet in a forward vortex flow (FVF) without interacting with the plasma. A smaller anode diameter (7 mm), however, leads to a more pronounced RVF, thereby increasing the interaction between the gas and the plasma. They proposed to increase "the fraction of gas passing through the plasma" as a general criterion for an improved performance.

In this work, we tested more electrode variations of length and diameter in both the cathode and anode, to further investigate this hypothesis. In an attempt to quantify the fraction of gas passing through the plasma for each of these designs, we define the plasma/reactor volume ratio as follows:

$$\frac{\text{Plasma}}{\text{reactor}}\text{ volume ratio} = \frac{(0.5 \cdot \text{arc diameter})^2 \cdot \text{arc length} \cdot \pi}{\text{reactor volume}} \quad \text{(F1)}$$

The plasma zone is simply considered as a static cylinder in the centre of the reactor. An arc diameter of 0.2 mm is estimated from the fast camera imaging data of Ramakers et al. [41]. The height is taken as sum of the cathode length, anode length and a cathode-anode distance of 1.75 mm. This plasma volume is then divided by the total reactor volume. Note that this is only a simple estimation of the plasma volume,

because the arc is not static, but it constantly reignites. Nevertheless, this ratio can give a first estimate of the fraction of gas passing through the plasma.

Table 1 gives an overview of all electrode combinations and their plasma/reactor volume ratio. The dimensions are specified in the names, and in the Supporting Information (SI) in section S2. A smaller anode diameter results in a larger plasma/reactor volume ratio, which is in line with the criterion of the fraction of gas passing through the plasma, indicating that this ratio is an acceptable definition. We considered more variations in electrode length and diameter. In general, we can see that a smaller cathode volume leads to a higher plasma/reactor ratio and we expect that more gas will interact with the plasma. This is also the case for the cone-shaped cathode, where the diameter narrows towards the top. For the anode length, we consider one very long design of 90 mm compared to 16 mm. For now, we assume that the plasma is elongated over the whole length in the plasma/reactor volume ratio, to be consistent with the other designs, although this is not necessarily true (as will be demonstrated later in the paper).

We also tested a number of electrode shapes differing more drastically from the standard case: the inserted anode configurations, as displayed in Table 2. They are elongated into the cathode reactor body and occupy nearly the entire volume. The gas still flows in as a wider upward vortex, but is now forced all the way to the top of the reactor body before going into the long outlet channel. If the plasma occupies the entire outlet channel, the gas should have a longer residence time in the plasma and cannot exit the reactor in a forward vortex flow. This also means that the plasma/reactor volume ratio should be even higher, but we used the same definition for consistency.

Besides the plasma/reactor volume ratio, we can also calculate the residence time based on the volume of each reactor. It will be interesting to compare the two, because they are not exactly the same. For example, a smaller cathode volume will have a higher plasma/reactor volume ratio, but a shorter residence time. We tested all the combinations at the same flow rate of 10 $L_s$min^{-1}, but also at a higher flow rate of 20 $L_s$min^{-1} to investigate the effect of a shorter residence time on the performance.

All variations were limited within the same outer shape of the electrode (dark grey) to guarantee a good fit in the surrounding reactor (light grey); hence, larger dimensions were not feasible. Smaller sizes were not possible either, since the gas volume would become too small for the flow rates of interest and the pressure would increase above safe levels.
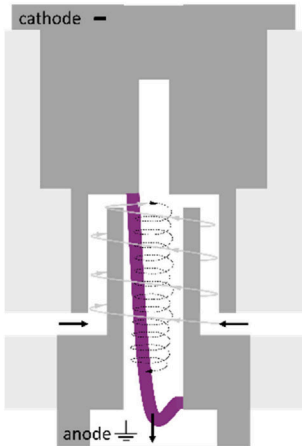
Table 1
Overview of all GAP electrode configurations evaluated in this work and the plasma/reactor volume ratio for each combination. The outer shape of the electrode is displayed in dark grey, while the white space represents the gas volume. The length and diameter of the electrode are specified in the electrode name in mm. Unless stated otherwise, the dimensions of the electrodes are drawn to scale. The "default" reactor design that was tested by Ramakers et al. [17] is the C_{L20_d18} and A_{L16_d7} combination (indicated in bold underlined and shown in Fig. 2).

Plasma/reactor volume ratio x 10^-3	Cathode →	C_{L10_d18}	C_{L20_d18}	C_{L30_d18}	C_{L20_d10}	$C_{L16\_d18\_cone}$
Anode ↓						
	$A_{L16\_d3.5}$	0.18	0.16	0.15	0.24	0.25
	A_{L16_d7}	0.16	**0.15**	0.14	0.22	0.22
	A_{L16_d14}	0.12	0.12	0.12	0.16	0.16
	A_{L90_d7} (not on scale)	0.39	0.33	0.29	0.42	0.45

Table 2
Overview of the inserted anode configurations evaluated in this work and the plasma/reactor volume ratio for each combination. The outer shape of the electrode is displayed in dark grey, while the white space represents the gas volume. The length and diameter of the electrode are specified in the electrode name in mm. The dimensions of the electrodes are drawn to scale. The picture in the right column illustrates how the inserted anodes fit into the cathode body, with schematic indication of the arc.

Plasma/reactor volume ratio x 10^-3	Cathode →	$C_{L16\_d18\_flat}$	Illustrative cathode-anode combination ↓
Anode ↓			
	$A_{insert\_L30\_d8}$	0.30	
	$A_{tapered\_insert\_L30\_d8}$	0.33	
	$A_{tapered\_insert\_L30\_d4}$	0.34	

2.3. Gas analysis

When using the NDIR, we use the following formula to calculate the conversion:

$$\chi = \frac{1 - y_{CO_2}^{out}}{1 + \frac{y_{CO_2}^{out}}{2}} \qquad (F2)$$

Where $y_{CO_2}^{out}$ is the output fraction of CO_2. This formula is valid since we only use CO_2 as an input gas. This formula inherently accounts for the gas expansion, and the derivation is given in the Supporting Information (SI, section S3).

The specific energy input (SEI), an important parameter to determine the energy efficiency, is defined as follows:

$$\text{SEI} \left[\text{kJ L}^{-1}\right] = \frac{\text{Plasma power [kW]}}{\text{Flow rate} \left[\text{L}_s \text{ min}^{-1}\right]} \cdot 60 \left[\text{s min}^{-1}\right] \qquad (F3)$$

With the flow rate expressed in L_s min^{-1} (litres standard per minute) with reference conditions at 20 °C and 1 atm.

The energy efficiency is defined as:

$$\eta \ [\%] = \frac{\chi_{CO_2}[\%] \cdot \Delta H_R^{\circ}[\text{kJ mol}^{-1}]}{\text{SEI} \left[\text{kJ L}^{-1}\right] \cdot 24.1 \ [\text{L mol}^{-1}]} \qquad (F4)$$

Where ΔH_R° is the reaction enthalpy for CO_2 splitting at standard conditions (i.e. 283 kJ/mol) and 24.1 L mol^{-1} is the molar volume defined at the same reference conditions of the flow rate (20 °C and 1 atm).

We performed every experiment three times, in order to apply a propagation of uncertainty to the results and calculate the error bars.

Fig. 3. (a) CO_2 conversion and (b) energy efficiency, presented as bars (left axis). The scatter plot represents the (a) plasma power and (b) SEI (right axis). The grouped bars represent the different cathode lengths (L10, L20, L30, see x-axis, with a fixed cathode diameter d18), while the bar colors represent the anode diameters (d3.5, d7, d14, see legend, with a fixed anode length: L16).

3. The effect of electrode shape on CO_2 conversion

In this section, we explore a variation of electrode configurations in the GAP in three series of experiments. All designs are tested for one condition (10 L_s min^{-1} and 0.4 A), measured in triplicates. For the influence of flow rate and current on the performance, we refer to earlier works about the GAP [17–21]. In this section, we present the results from least to most different from the "default" reactor design with C_{L20_d18} and A_{L16_d7} that was tested by Ramakers et al. [17].

3.1. Variation in cathode length and anode diameter

In the first series of experiments, we compare different cathode lengths in combination with various anode diameters. The cathode diameter and anode length are kept constant. These designs are most in line with previous work [17], only the dimensions are different. Fig. 3 represents the CO_2 conversion and energy efficiency as a function of the cathode length, for the different anode diameters. The power and SEI are also plotted (right y-axes).

For the middle cathode (C_{L20_d18}) we observe the same trend as Ramakers et al. [17] When the outlet diameter in the anode is reduced from 14 to 7 mm, the conversion increases from 6.34 ± 0.39 % to 7.99 ± 0.39 %. When the outlet decreases even further to 3.5 mm, the conversion rises further to 9.32 ± 0.39 %. This same trend holds for the shorter cathode (C_{L10_d18}) with a marginally smaller conversion. Yet, the power input for this cathode is much higher, resulting in a much lower energy efficiency. For the longest cathode (C_{L30_d18}) the conversion is slightly higher. Similar to the shorter cathodes, the CO_2 conversion increases from 6.81 ± 0.39 % for the 14 mm anode to 9.66 ± 0.39 % for the 7 mm anode; however, we do not see a similar rise for the smallest anode (9.64 ± 0.39 %). The conversion for both the 3.5 and 7 mm anodes is the same for the longest cathode, but the smallest anode still performs slightly better in terms of energy efficiency (29.45 ± 1.20 % vs. 26.94 ± 1.17 %; see Fig. 3(b)), due to the lower SEI.

Since we used the same input current of 0.4 A for different electrode designs, the resulting plasma power is not constant. This likely influences the gas temperature and hence, the CO_2 conversion. However, we cannot directly control the temperature of the plasma, nor the exact plasma input power, since this depends on the plasma characteristics. But we can influence the plasma characteristics by changing the electrode design, which is exactly the goal of this work. We believe it is a suitable approach to optimise the electrodes by comparing the energy efficiency, since it accounts for the conversion at a certain specific energy input.

A smaller anode diameter and a longer cathode are clearly beneficial for the performance in terms of CO_2 conversion and energy efficiency. The fact that a smaller anode diameter results in a higher conversion meets our expectations, since the reverse vortex flow is more pronounced, yielding better insulation from the walls. In addition, a longer cathode increases the plasma length, thereby increasing the residence time. However, it should be noted that these dimensions are the limit for the current reactor. We cannot decrease the anode diameter much further; otherwise, the overpressure in the reactor would reach a dangerous level. Likewise, we cannot elongate the cathode further. This would require much higher powers to sustain the plasma and we currently do not have such a power supply. In addition, previous work regarding the dual vortex plasmatron [24], has shown that it is not simple to elongate a plasma and provide sufficient power. Trenchev et al. did not obtain a significantly higher conversion and energy efficiency than in this GAP reactor. We summarise these findings in a critical comparison in Section 4 below.

3.2. Variation in anode length, cathode diameter and cathode shape

In the second series of experiments, we test other variations to the default electrode design. The two remaining dimensions that were not
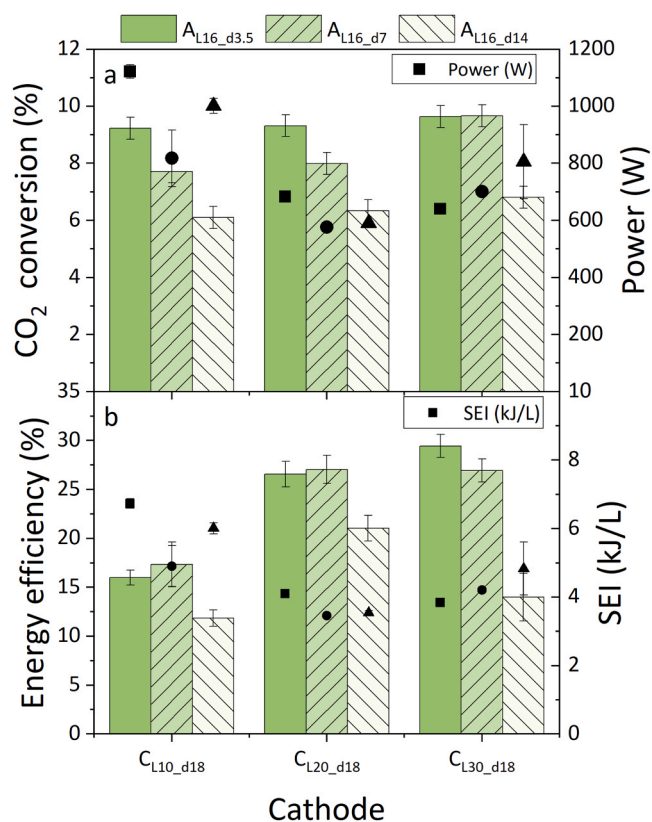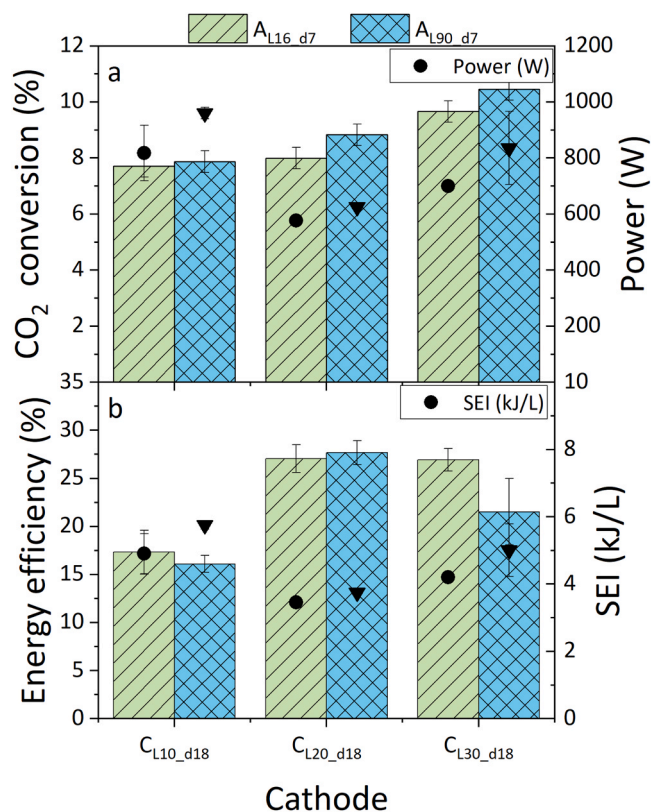
Fig. 4. (a) CO_2 conversion and (b) energy efficiency, presented as bars (left axis). The scatter plot represents the (a) plasma power and (b) SEI (right axis). The grouped bars represent the different cathode lengths (L10, L20, L30, see x-axis, with a fixed cathode diameter d18), while the bar colors represent the anode lengths (L16 and L90, see legend, with a fixed anode diameter: d7).
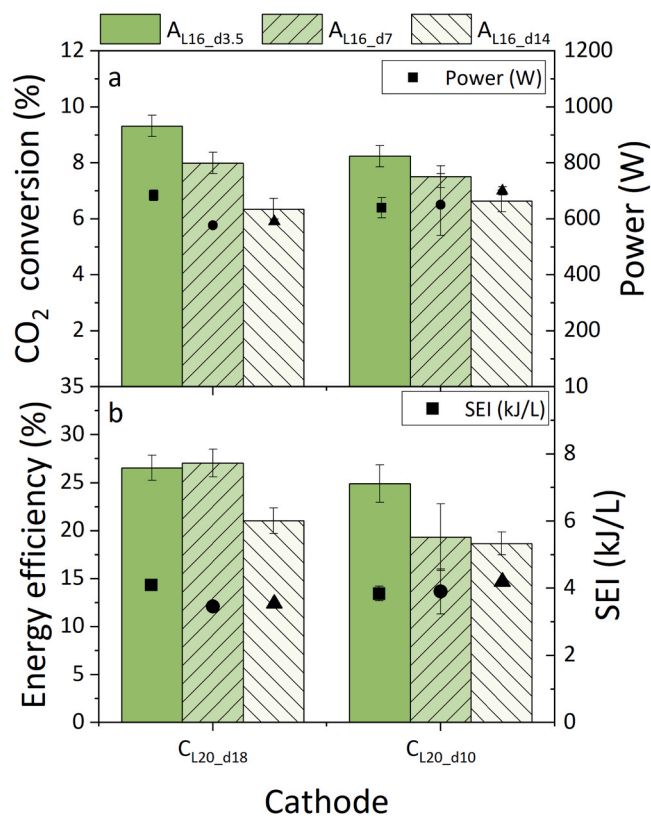

Fig. 5. (a) CO_2 conversion and (b) energy efficiency, presented as bars (left axis). The scatter plot represents the (a) plasma power and (b) SEI (right axis). The grouped bars represent the different cathode diameters (d18 and d10, see x-axis, with a fixed cathode length L20), while the bar colors represent the anode diameters (d3.5, d7, d14, see legend, with a fixed anode length: L16).

yet tested in Section 3.1, i.e. the anode length and cathode diameter, will be compared to the default results. In addition, we also tested a more novel shaped cone cathode where the cathode diameter narrows at the top.

3.2.1. Anode length

We increased the anode length from 16 mm to 90 mm, to investigate whether this could elongate the plasma zone and thus enhance the conversion. The results are displayed in Fig. 4, for the three different cathode lengths, with an anode diameter of 7 mm. Although we demonstrated in the previous section that the smaller diameter of 3.5 mm is more beneficial for the conversion, we chose to make our new designs starting from the standard electrode dimensions.

We observed that the design with a longer anode needs a longer time to reach the steady state. When following the real time concentrations on the NDIR, this configuration reaches a stable value after about 7 min, while the shorter anode needs only 2 min to reach a stable output concentration. Clearly, the longer anode warms up due to the hot gas that exits the reactor. This results in a slightly higher conversion for all three cathode lengths and the difference is most pronounced in the longest cathode. However, the power is generally higher and thus the energy efficiency is comparable to or even lower than the basic design (see Fig. 4(b)), which can be attributed to heating losses.

Another reason for the slightly higher conversion can be the more elongated plasma in the longer anode. These results are in line with the fundamental mechanisms that were investigated by Xu et al. [44] in a rotating gliding arc in air. When they added an extension tube to their rotating gliding arc reactor, the gliding arc became longer and the regeneration frequency lower. A similar effect was observed by Jardali et al. [13] for NOx production. When the arc is elongated towards the

anode outlet in the steady mode, the NO_x concentration is much higher compared to the shorter arc in the rotating mode. A more elongated plasma could explain the slightly higher CO_2 conversion in this work, however, we observed no electrode damage on the elongated anode, compared to clear signs of arc attachment in the shorter anode. This indicates that the arc is not significantly elongated in the anode, which might explain why the difference in performance is so small.

3.2.2. Cathode diameter

For the basic cathode length (20 mm), we reduced the cathode diameter from 18 to 10 mm. The plasma zone in the narrower cathode occupies a larger fraction of the reactor body. Hence, we might expect that the fraction of gas going through the plasma would increase, which may yield a better performance, as assumed in previous work [17,40]. The results are given in Fig. 5, for the three different anode diameters.

The CO_2 conversion is not higher, but even slightly lower in the smaller cathode compared to the wider standard cathode, while it consumes a bit more power. As a consequence, the energy efficiency is lower as well, indicating that the heating loss to the walls is perhaps more significant for the performance than the volume fraction occupied by of the plasma in the reactor (affecting the gas fraction treated by the plasma).

This is in contrast to the results of Trenchev et al. [25] for an APGD, where reactor confinement gave three times higher CO_2 conversion (see also Section 1). However, in the APGD, the difference in volume was very large. In addition, the confined design also allowed to use three times lower CO_2 flow rate for similar power (due to the groove in the cathode, yielding efficient cooling), and thus three times higher SEI, explaining the three times higher CO_2 conversion. In the basic GAP design, the reactor body (cathode) diameter is already quite small, so
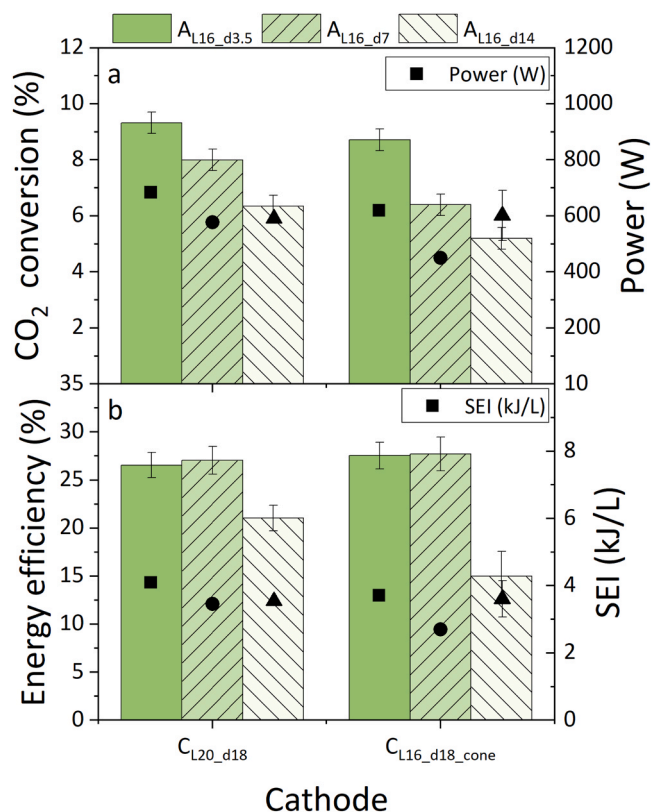
Fig. 6. (a) CO_2 conversion and (b) energy efficiency, presented as bars (left axis). The scatter plot represents the (a) plasma power and (b) SEI (right axis). The grouped bars represent the different cathode shapes (default and cone, see x-axis), while the bar colors represent the anode diameters (d3.5, d7, d14, see legend, with a fixed anode length: L16).

further confinement does not bring any improvement. Anyway, comparing design improvements in the GAP and APGD is difficult, because of the different plasma characteristics. In the APGD, the plasma is characterized by wall stabilization, while this does not happen for the arc in the GAP reactor that is stabilized by the flow. Moreover, the heat transfer through the walls is different (i.e. ceramic for the APGD, vs steel for the GAP).

3.2.3. Cone-shaped cathode

Instead of a cylindrical cathode, we also tested the effect of a cone-shaped cathode. By reducing the upper radius of the cathode, the reactor body narrows down towards the upper end, and might improve the contact between the cold gas and the plasma zone. Fig. 6 shows the results, for the three different anode diameters, in comparison to the basic GAP design. The length of the cone (16 mm) is slightly shorter than the basic design, but we demonstrated earlier in Fig. 3 that the conversion is very similar for the two basic cathodes with a length of 10 and 20 mm.

The overall CO_2 conversion is somewhat lower in the cone-shaped cathode compared to the cylindrical cathode. The energy efficiency is comparable for the two smallest anodes (3.5 and 7 mm), but smaller for the largest anode (14 mm). These findings are in line with the result from the smaller cathode diameter. It appears that the fraction of gas passing through the plasma is less suitable as a criterion for improving the reactor design, which will be discussed in more detail in 4.1. It seems that a larger total reactor volume is more beneficial for the GAP, especially in combination with smaller anode diameters. This can facilitate a more pronounced reverse vortex flow and enhance the interaction between the hot plasma core and the cool surrounding edge to minimize the heat losses. Overall, these results indicate that the original GAP
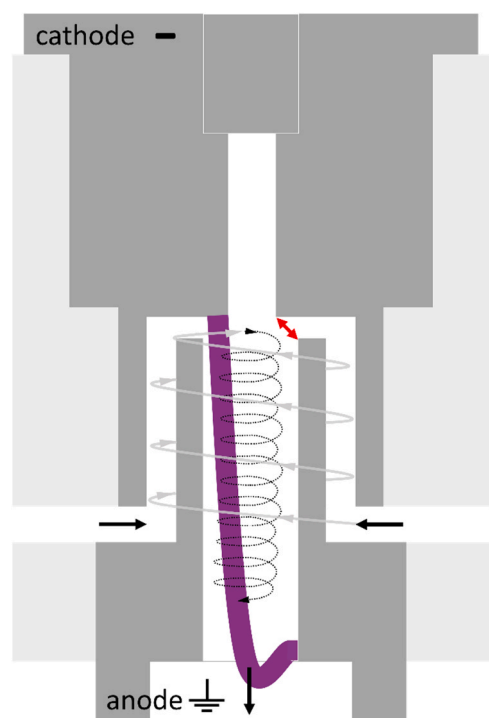
Fig. 7. Schematic 2D representation of the GAP reactor with the inserted anode into the cathode reactor body. Dark grey indicates the cathode and anode electrodes, light grey represents how they fit into the reactor body. The white space represents the gas volume. The up- and downward vortex of the gas is schematically represented as the outer and inner vortex (grey and black), respectively. The gas flows in through six tangential inlets from the side, goes inside the reactor volume and then flows out through the anode. In the ideal case, the arc discharge would be formed between the cathode and the furthest anode point at the outlet, so that it fills the entire anode outlet, as schematically presented in purple. However, the red arrow indicates another plausible case, with a small rotating arc at the top of the inserted anode, such that the arc does not fill the entire anode outlet.

reactor design [16] was already quite optimised.

In the next part, we investigate a more drastic change to the standard electrode design, i.e. the so-called inserted anodes. Note that the design idea started again from the criterion of increasing "the fraction of gas passing through the plasma". Although we already demonstrated in this section that this might not be suitable, the inserted designs can help us to understand this criterion better and whether more drastic design changes might have a larger effect on the performance.

3.3. Inserted anodes to increase plasma-gas interaction

The third series of experiments involves a more novel variation of the GAP design, where the anode outlet is elongated and inserted into the cathode reactor body (Fig. 7). When the gas is flowing in the wider upward vortex, it is forced all the way to the top of the (cathode) reactor body and it returns in the narrow downward vortex, inside the long (anode) outlet channel. When the plasma arc would be formed between the cathode and the furthest anode point at the outlet, it would occupy the entire outlet channel (purple) and the gas would have a longer residence time in the plasma. The results are displayed in Fig. 8 for the three different "inserted" anode designs: a cylindrical shape (diameter 8 mm), a tapered shape with a wider top (8 mm) and smaller bottom (2 mm) and another tapered shape with a smaller top (4 mm) and smaller bottom (2 mm). Again, the results are compared to the basic GAP design with three different anode diameters.

Clearly, the overall conversion with the three different inserted anodes is lower. The $A_{insert\_L30\_d8}$ with the wider outlet is significantly
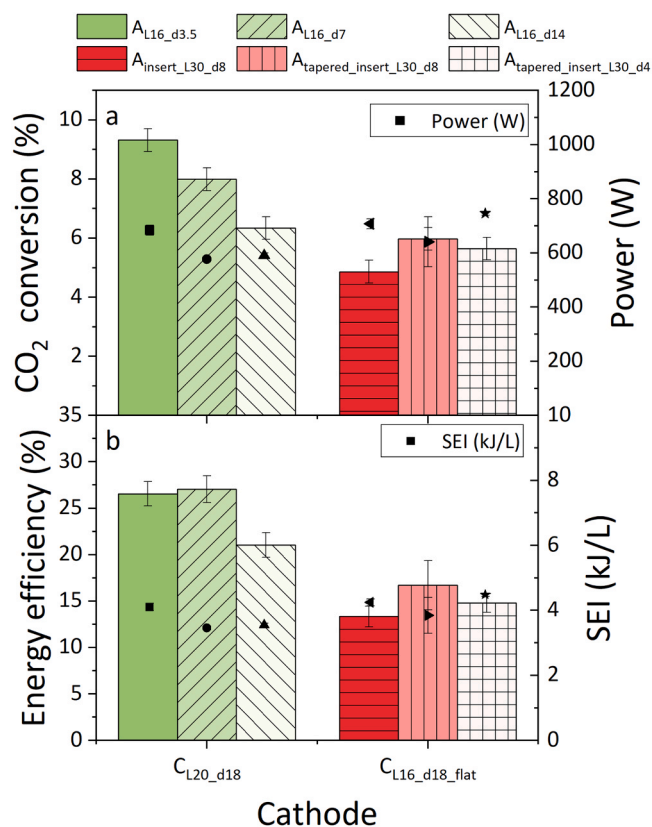
Fig. 8. (a) CO_2 conversion and (b) energy efficiency, presented as bars (left axis). The scatter plot represents the (a) plasma power and (b) SEI (right axis). The grouped bars represent the different cathodes (default C_{L20_d18} and inserted $C_{L16\_d18\_flat}$, see x-axis), while the bar colors represent the anode specifications (see legend).

lower than all results of the basic configuration, with a CO_2 conversion of only 4.86 ± 0.38 %. The two inserted anodes with a smaller outlet perform slightly better, but still much worse than for the basic anode designs. The difference is even larger for the energy efficiency, with significantly lower values, even when compared to the worst basic design. In addition, it was more difficult to obtain a stable plasma in these inserted anodes and they extinguished easily when using a different power supply (e.g. the AC current source power supply from AFS used by Girard-Sahun et al. [45]).

These results are in line with our conclusions from the cathodes with the smaller diameter: again the criterion to increase the fraction of gas passing through the plasma seems not applicable here. However, it is likely that the arc is not elongated in the whole anode outlet at the conditions under study. If the arc forms at the shortest point between the cathode and the anode (red arrow in Fig. 7) and the plasma does not stabilise in the centre, the plasma zone is very small. This could also explain the low performance and bad plasma stability in these inserted anode configurations. Considering their overall lower performance and difficulty to stabilise the plasma, we do not include these electrodes in the summary of all electrode variations in Section 4.

In this section, we focused on the performance in terms of CO_2 conversion and energy efficiency as a function of the various design parameters. However, to better understand the performance results, it is useful to study the plasma characteristics. Based on our oscilloscope measurements, we analyse the voltage measured for each design, in the SI section S4. The voltage variations as a function of time demonstrate that the arc is continuously attaching and detaching, as expected for a gliding arc plasma, and in line with earlier observations by our group with fast camera imaging [41]. Furthermore, we analyze the time-averaged voltages as an indication of the arc length and cooling

effects. We can conclude that the arc length (outside the reactor) affects the performance. In addition, our analysis reveals that post-plasma recombination of the products (and thus post-plasma quenching of the gas to remediate this [46–48]), as well as plasma stability, appear more important than plasma-gas interaction in the reactor. However, this analysis of the average voltage remains only indicative, since more detailed in-situ optical diagnostics to validate this analysis was out of scope for this work.

4. Overall performance

In the previous section, we discussed the performance of each series of electrode designs and we reflected on how changes in the plasma can explain the different results. In this section, we first make an overall comparison based on the plasma/reactor volume ratio, and subsequently we discuss the residence time as a more general parameter. Finally, we summarise the energy efficiency as a function of the CO_2 conversion to give an overview of all the results in this work.

4.1. Plasma/reactor volume ratio

We calculated the plasma/reactor volume ratio as a simple metric for the fraction of gas passing through the plasma and we present its relation to the CO_2 conversion in Fig. 9. Both graphs display the same data, but are grouped for each cathode (a) or anode (b). The schematic representations of these electrodes are given on each side, indicated by the symbol in the graph. As intended, a smaller cathode volume leads to a larger plasma/reactor volume ratio. Also the C_{L20_d10} and $C_{L16\_d18\_cone}$ have higher ratios than the basic cathode, which was exactly the idea behind these designs. A longer anode also increases the plasma/reactor volume ratio, if we assume that the plasma fills the entire outlet.

It is clear from Fig. 9 that the CO_2 conversion does not only depend on the plasma/reactor volume ratio. Instead, we observe different trends, that are not always clear. Ttwo of them can be more clearly distinguished, as indicated by the black dashed arrows. First, when we consider the same cathode, like C_{L20_d10}, the CO_2 conversion increases for a larger plasma/reactor volume ratio (Fig. 9a: dashed arrow 1), which we obtain by decreasing the anode diameter (Fig. 9b). This is in line with observations in previous work and the basis for the hypothesis that increasing the fraction of gas passing through the plasma will improve the performance. We see a different trend, however, when we consider a single anode, like A_{L90_d7}, indicated by dashed arrow 2. The CO_2 conversion decreases for a larger plasma/volume ratio (Fig. 9b), which we achieve with a smaller cathode volume (Fig. 9a). This is quite interesting, since a larger plasma/reactor volume ratio implies that the gas is heated more uniformly in the reactor, yet: the conversion is lower. This confirms that the CO_2 conversion in this reactor is not solely due to the higher temperature, but that the mixing with the cool outer vortex also plays a role (see below).

Since the electrode design will change the plasma characteristics, the different power inputs might explain the trends in conversion. However, when we plot the power input as a function of the plasma/reactor volume ratio in Fig. 10, we see no clear relation between both. Most designs have a power between 550 and 750 W, and the configurations that fall outside of this range do not necessarily result in a higher or lower conversion in Fig. 9. The power input of $C_{L10\_d18}A_{L16\_d3.5}$ for example is very high, above 1 kW, but the CO_2 conversion is only about 9 %, just like other designs with moderate powers of 750 W. Hence, the power input cannot explain the trends in conversion.

To summarise the performance, we believe it is most suitable to compare the energy efficiency of the different designs, because this accounts for the CO_2 conversion at a specific energy input. Fig. 11 displays the energy efficiency as a function of the plasma/reactor volume ratio.

There is no general trend between the energy efficiency and the plasma/reactor volume ratio. Although this parameter is able to explain some patterns in the conversion, it does not capture the different plasma
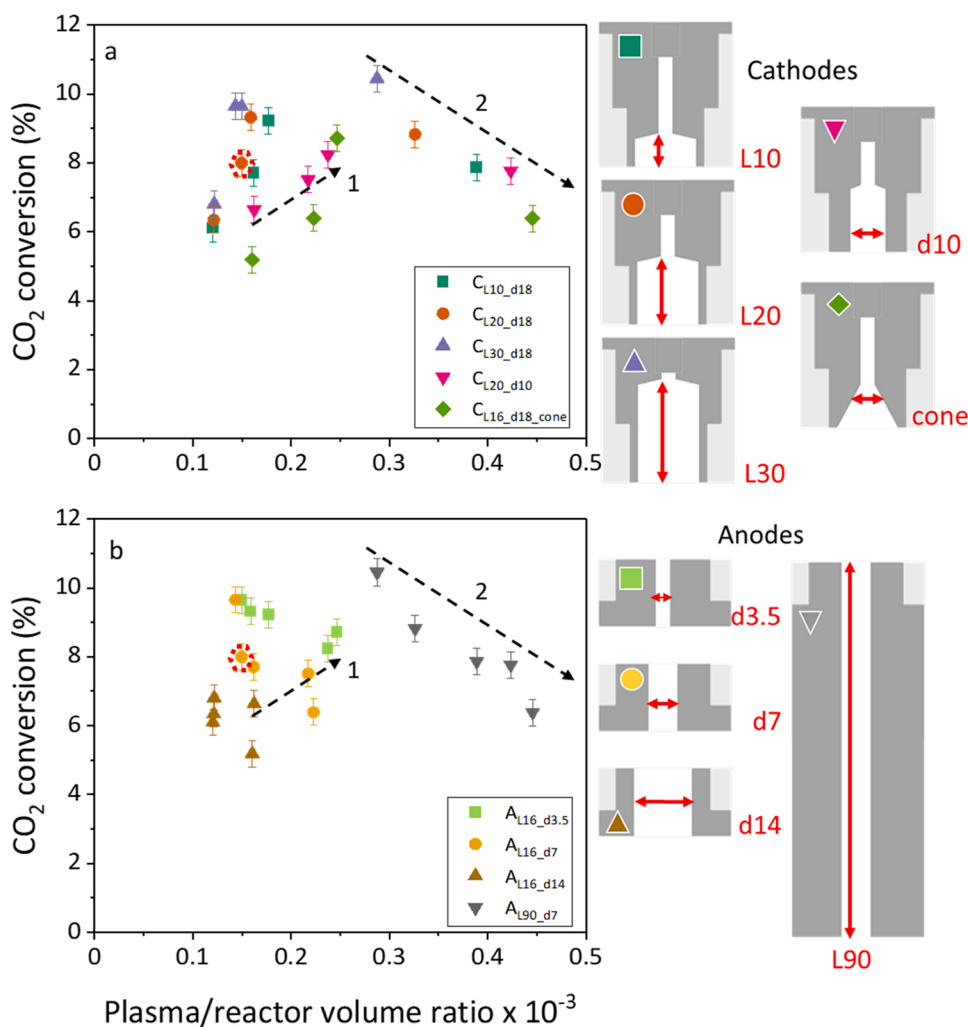
Fig. 9. CO$_2$ conversion as a function of the plasma/reactor volume ratio for all electrode combinations (except the inserted anodes): (a) grouped for each cathode and (b) grouped for each anode. The schematic representations are displayed on the right, with a red double arrow to indicate the most important characteristic dimension, also written next to the scheme. The red dotted circle in the graph indicates the basic combination, C$_{L20\_d18}$A$_{L16\_d7}$. The black dashed arrows in the graphs highlight two different trends when considering (1) a single cathode, e. g. C$_{L20\_d10}$, or (2) a single anode, e.g. A$_{L90\_d7}$.

characteristics that will alter the power for each design as seen in Fig. 10.

Possibly, the plasma/reactor volume ratio, as defined in this work, is not a good definition for the fraction of gas passing through the plasma. As mentioned in Section 2.2, only a very simple formula is used, based on a simple static cylinder for the arc, which does not reflect reality, due to the turbulent vortex flow pattern and the reignition of the rotating arc. Therefore, we conclude that the simple formula defined in Section 2.2, to estimate the "fraction of gas passing through the plasma", is not suitable to improve the performance.

Instead, we believe the results in this work should be interpreted more in general. It is not necessarily the fraction of gas passing through the plasma that plays a crucial role, but it is the interaction between the hot plasma core and the cooler outer edge. Indeed, previous work [17, 40] demonstrated more in general that a smaller anode diameter leads to a more pronounced reverse vortex flow. The forward (outer) vortex flow of the cooler gas provides an isolation for the reverse (inner) vortex of the hot gas passing through the arc and limits heat losses to the walls. Both forward and reverse vortex flow have their function in this reactor. When we decrease the cathode diameter in this work, the role of both separate vortices would disappear because the arc occupies most of the reactor volume, and this appears to be detrimental for the performance.

The presence of a hot core surrounded by the cooler gas has two advantages. Firstly, the cool flow reduces the heat losses to the walls by improving the convective cooling of the hot plasma core, which is the main incentive for studying the reverse vortex flows in plasma [49]. Secondly, the chemistry is enhanced as well, which was recently investigated by van den Bekerom et al. [50] and van de Steeg et al. [51] in microwave (MW) plasmas. They concluded that the temperature gradients drive fast core-periphery transport and mixing, which minimizes CO losses and optimises the use of O radicals in the O + CO$_2$ reaction, further enhancing the CO$_2$ conversion. In case of the basic GAP reactor, where the arc is also located in the centre, we can expect that this interaction between the hot core and surrounding cooler edge is important as well.

One disadvantage is that we cannot quantify this interaction in the same manner as we did for the plasma/reactor volume ratio. Furthermore, the energy efficiency shows no clear correlation as a function of the design parameters, indicating that the performance might be limited independent of the electrode design. We investigate this in more detail, by comparing our results to different plasma reactors in Section 5.1.

Finally, we did not include the unstable inserted anodes from Section 3.3, even though these designs were made for the optimal plasma-gas interaction. Their low conversion indicates that plasma stability is more important than the plasma-gas interaction.

4.2. Residence time

The residence time is a more general parameter to summarize the variety in electrode dimensions and shape. We expect from traditional reaction engineering that a longer residence time increases the CO$_2$ conversion and therefore we plot the results in Fig. 12. Some results with a higher flow rate of 20 L$_s$ min^{-1} are also included, because they have a shorter residence time; these are discussed in more detail in the SI
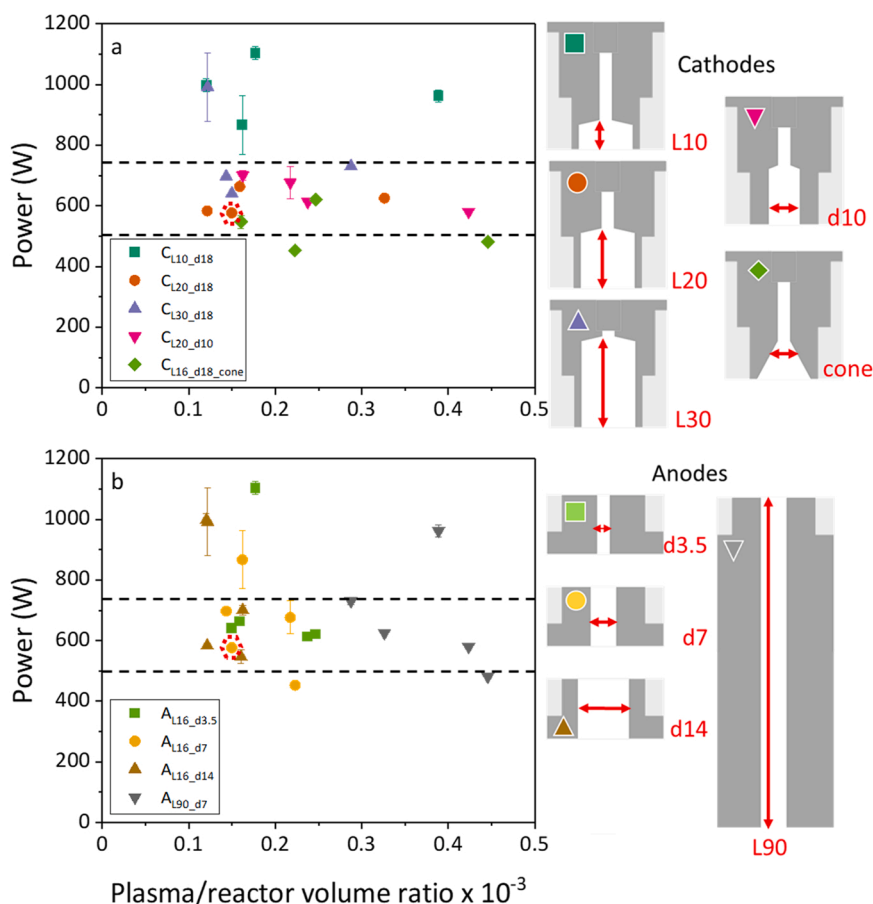
Fig. 10. Power as a function of the plasma/reactor volume ratio for all electrode combinations (except the inserted anodes): (a) grouped for each cathode and (b) grouped for each anode. The schematic representations are displayed on the right, with a red double arrow to indicate the most important characteristic dimension, also written next to the scheme. The red dotted circle in the graph indicates the basic combination, $C_{L20\_d18}A_{L16\_d7}$. The black dashed lines indicate the most common power range for most designs.

(section S5).

For each anode in Fig. 12b, the residence time increases when it is combined with a larger cathode of Fig. 12a and as a result, the CO_2 conversion increases accordingly, as indicated for the A_{L90_d7} anode. Furthermore, the combination $C_{L30\_d18}A_{L90\_d7}$ has the longest residence time and also the highest CO_2 conversion. However, both graphs clearly demonstrate that the residence time is also not the only parameter that plays a role. A smaller anode diameter will result in a higher CO_2 conversion at the same residence time as wider anodes. Indeed, the $C_{L30\_d18}A_{L16\_d14}$ combination (indicated by the black dotted square in Fig. 12) has the second highest residence time, but the CO_2 conversion is significantly lower than most results with smaller anode diameters.

When considering the energy efficiency in Fig. 13, we again observe no general trend between the residence time and the energy efficiency. Just like for the definition of plasma/reactor volume ratio, the residence time does not capture the effect of the different plasma characteristics.

Indeed, while the conversion generally increases for a longer residence time, the specific energy input increases simultaneously. As a result, the energy efficiency reaches the same maximum of 30 % for a wide range of residence times. At a constant flow rate, like in these experiments, a larger reactor can lead to a higher power input and a larger plasma volume, but the balance between conversion and power input remains the same. Even for a higher flow rate, the energy efficiency reaches the same maximum, despite the low conversion.

Clearly, the residence time is not a suitable criterion to optimise the performance either. This was also addressed in our previous work in an atmospheric pressure glow discharge [52]. Simply elongating the discharge is not sufficient to improve the performance, especially when chemical equilibrium is reached quickly, but placing reactors in series can help to improve the conversion. Such alternative solutions, beyond the internal reactor design, are discussed with a literature review in

Section 5.

We conclude that there is not one simple parameter that defines the optimal design, due to the complex interaction between the gas flow and the plasma behaviour. These underlying mechanisms could be further elucidated with a fluid dynamics model, as was done previously for the anode diameter by Ramakers et al. [17]. However, since we observe more subtle variations in the experimental conversion in this work, we have to improve the previous models developed in our group, by a fully coupled description of the gas flow dynamics and plasma behaviour. This is quite challenging, and out of scope for this work, but it will be subject of future work.

4.3. Overview of all results in this work

All combinations of Section 3 are summarised in Fig. 14. The energy efficiency is plotted as a function of CO_2 conversion to give an overview of the two most important performance parameters. Again, both graphs display the same data, but are grouped for each cathode (a) or anode (b).

Clearly, changing the electrode design has a large influence on the performance. The design with highest energy efficiency (i.e. 30 %, for a conversion of 9.5 %) is the combination of the longest cathode (C_{L30_d18}) with the smallest anode diameter ($A_{L16\_d3.5}$). On the other hand, the CO_2 conversion is slightly higher (i.e., 10.5 %) if we combine the same (longest) cathode (C_{L30_d18}) with the longest anode (A_{L90_d7}), but the energy efficiency here is lower (i.e., 21 %), attributed to the heat losses to the walls of the anode outlet.

Equally important are the results that are not shown here, i.e. the electrode shapes that resulted in an unstable plasma. Indeed, the electrode design has a fundamental effect on the stability of the plasma. Some shapes did not result in a stable plasma, either due to quick electrode damage or due to the poor coupling with the power supply,
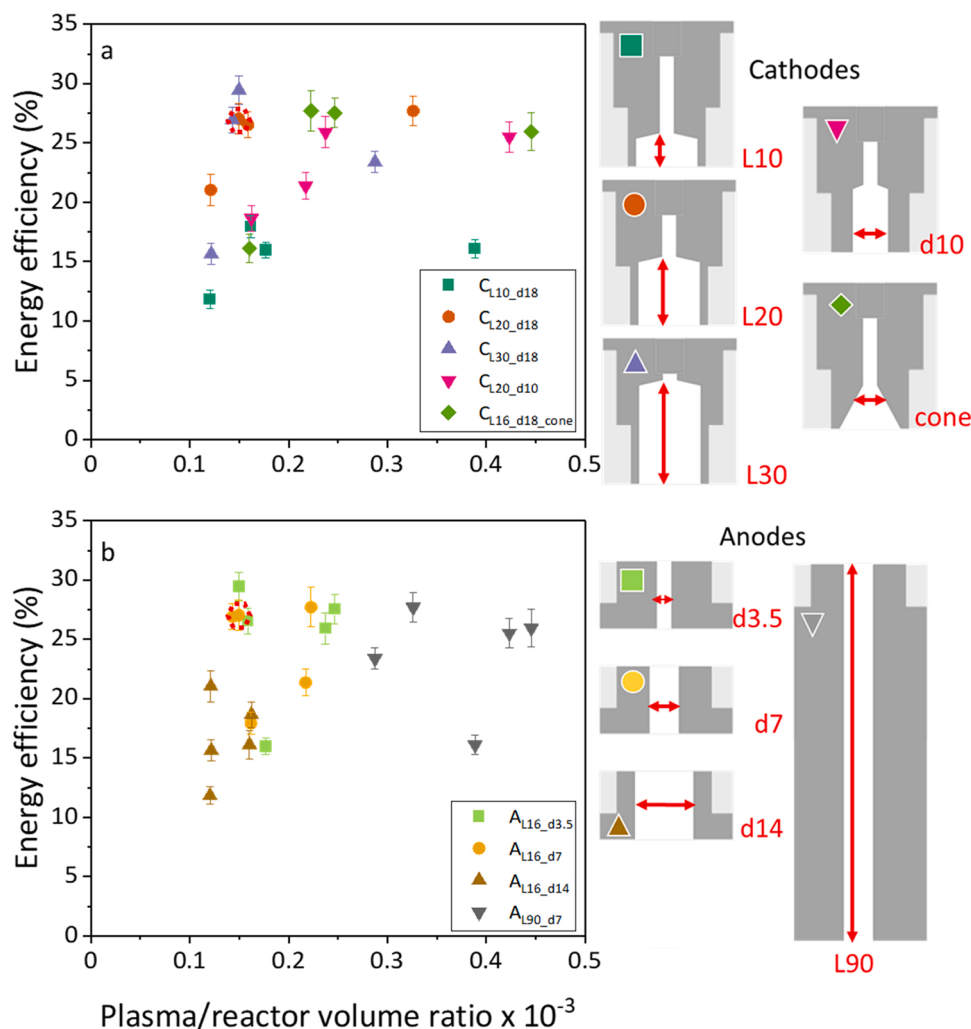
Fig. 11. Energy efficiency as a function of the plasma/reactor volume ratio for all electrode combinations (except the inserted anodes): (a) grouped for each cathode and (b) grouped for each anode. The schematic representations are displayed on the right, with a red double arrow to indicate the most important characteristic dimension, also written next to the scheme. The red dotted circle in the graph indicates the basic combination, $C_{L20\_d18}A_{L16\_d7}$.

resulting in too much electromagnetic interference (more details in SI, section S6) [53]. We know that the optimisation of the electrode design and the characteristics of the power supply are inherently intertwined, yet it is not straightforward to improve this coupling.

Some criticism is justified here: in spite of the large variations in performance for the different designs, there is no large improvement compared to the basic GAP design, even for the best designs shown above. Many electrodes perform worse than the basic design, which indicates that the original GAP reactor design [16] was already quite optimised, and only varying the electrode dimensions does not lead to significant improvements. Furthermore, the heat loss to the walls is an important factor that could explain the bad performance of the designs with a smaller reactor volume, i.e., smaller cathode diameter or cone-shaped cathode (C_{L20_d10} and $C_{L16\_d18\_cone}$). This heat insulation effect was an important incentive to study the reverse vortex flow in the basic GAP design in the first place, and here we only confirm that this effect is more pronounced in the wider cathodes. In addition, the wider cathodes allow the arc to be more concentrated in the centre, i.e., a hot plasma core surrounded by a cooler region. This enables fast core-periphery transport and mixing, minimizing CO losses upon recombination, and optimising the use of O radicals to further react with unconverted CO_2, as demonstrated in MW plasmas by van den Bekerom et al. [50] and van de Steeg et al. [51].

Further optimisation of the performance might be possible by

tweaking the power supply, although one might wonder whether the results will be different when the resulting plasma has similar discharge characteristics. In summary, our results are not significantly better than previous work on CO_2 conversion in the basic GAP reactor [17]. Would it then be better to investigate a completely new design? We discuss the answer to this question in the next section.

5. Comparison to the state-of-the-art

5.1. Comparison to other warm plasmas

We first compare different warm plasma reactors from our lab in Table 3, while we discuss a broader comparison in Section 5.2 below. All these plasmas in Table 3 operate at relatively high temperature (2500–3500 K inside the plasma), higher than a DBD plasma (300–400 K) [54]. In addition, there is physical contact between the plasma and the electrodes, which is not the case for MW and inductively coupled radio-frequency (ICP-RF) reactors. Most importantly, they all operate at atmospheric pressure for pure CO_2 conversion.

Despite the completely different reactor designs and operating conditions (power and flow rate), the performance of these warm plasmas is very similar, yielding a maximum CO_2 conversion around 10 % for a maximum energy efficiency around 30 %. They all seem to bump into the same limits as the GAP studied in the present work, where the
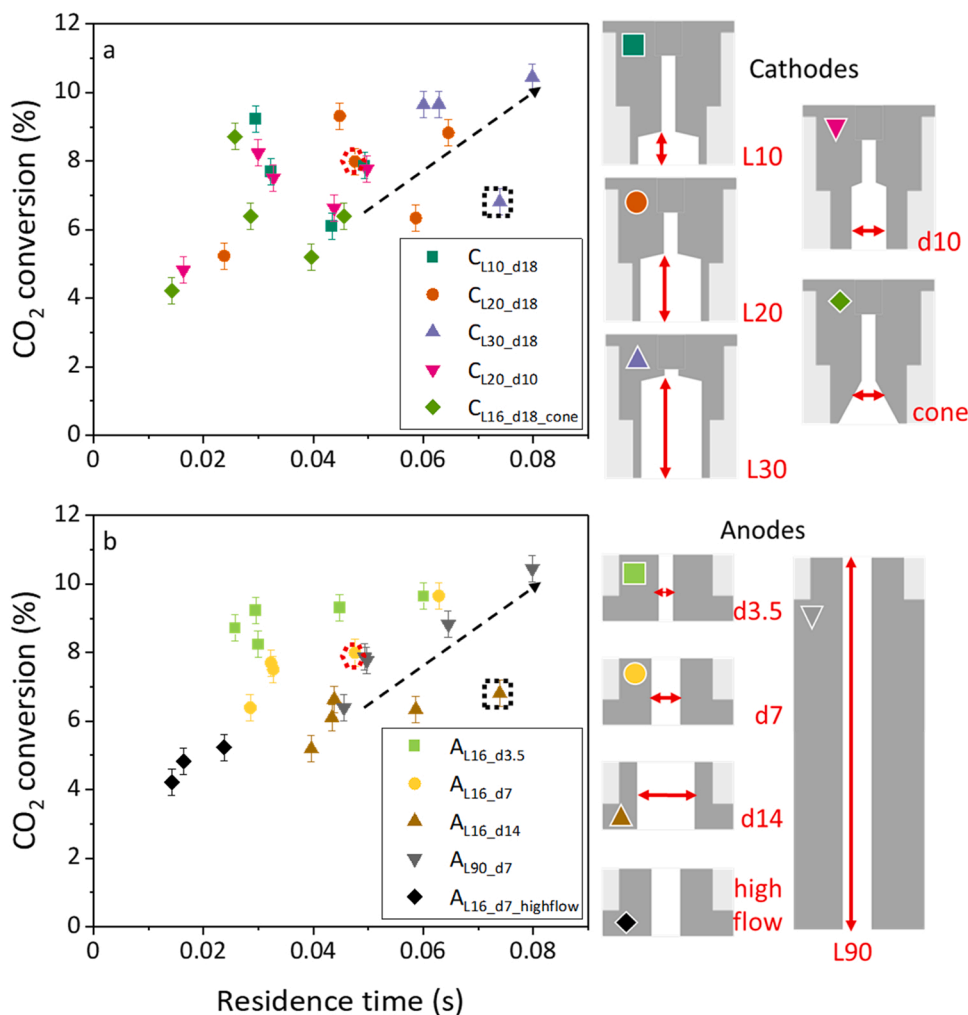
Fig. 12. CO_2 conversion as a function of residence time for all electrode combinations (except the inserted anodes): (a) grouped for each cathode and (b) grouped for each anode. The schematic representations are displayed on the right, with a red double arrow to indicate the most important characteristic dimension, also written next to the scheme. The red dotted circle in the graph indicates the basic combination, $C_{L20\_d18}A_{L16\_d7}$. The black dashed arrow in the graph highlights the trend when considering a single anode, e.g. A_{L90_d7} and the black dotted square highlights the $C_{L30\_d18}A_{L90\_d7}$ configuration that has the second highest residence time.

conversion is at maximum 10 % for the "best" designs. Some conditions with higher energy efficiency are possible, e.g. at higher flow rates, but this results in such low CO_2 conversion that it is not interesting from an industrial point of view, as investigated by van Rooij et al. [56]. From these comparisons, it appears that these "warm plasmas" (high temperature, contact between electrode and plasma, and for pure CO_2) have a certain limit in performance, independent of the reactor design. Even without contact between electrodes and the warm plasma (e.g. MW reactors), the performance is comparable at atmospheric pressure, as discussed in more detail below.

The high atmospheric pressure seems to play a key role. A higher power density (i.e. SEI) leads to a higher conversion, but then the discharge will contract due to the higher pressure, which reduces the amount of gas that is passing through the plasma. Wall stabilisation is one way to increase the plasma volume, such as in the confined APGD [25], but heat losses to the walls decrease the energy efficiency. Flow turbulence and flow rate also increase the plasma volume, but only in certain configurations, such as the RVF in the GAP reactor of this work. The longer afterglow we observe at higher flow rates, opposite to the classical 2D gliding arc discharge where the plasma contracts faster, confirms the role of turbulence. Finally, in low-pressure plasmas, the contraction of the discharge is not as strong and the plasma can occupy a larger volume at higher SEI. The latter, together with the possibility of vibrational-induced dissociation, may explain why they often show good performance. Note that we do not consider DBD plasmas here, since they operate in a much different regime as discussed below in 5.2.1.

Overall, there is not one explanation for the limit in performance. We

know that the total energy that goes into the reactor is divided over (i) the workload needed to sustain the plasma in the presence of a strong gas flow (i.e., contraction of the plasma), (ii) work in emitted radiation, (iii) dissipated heat, (iv) heating of the electrodes and finally (v) chemical reactions (including effects of quenching after the reactor, but also reactions due to mixing of the hot plasma core and the cold outer vortex). It is clear that plasma-based CO_2 conversion is complicated, and thus, there is not one simple parameter or experimental condition that defines the optimal plasma reactor design. Therefore, we discuss other strategies to enhance the performance in the next section.

5.2. Comparison to all CO_2 plasma reactors

Fortunately, there are other plasma conditions and strategies to improve the performance of plasma reactors for CO_2 conversion. Numerous examples in literature go beyond the results of this work, which can be found in an extensive literature review by Snoeckx and Bogaerts in 2017 [15]. They summarised the energy efficiency as a function of CO_2 conversion for all types of plasma reactors. We updated this figure with more recent literature (published since 2016–2017) in Fig. 15, for MW reactors [37,46,50,57–79], gliding arc plasma reactors [24,28,31,80–86], DBD plasmas [87–132], plasmas with a post-plasma carbon bed [45,133–137] and other plasma types (i.e. spark discharge [138], glow discharge [139–145], atmospheric pressure glow discharge [25,52,146,147], thermal torches [148,149] and nanosecond pulsed discharges [150,151]). It is important to note that we only included papers on pure CO_2 splitting that report both the conversion and energy
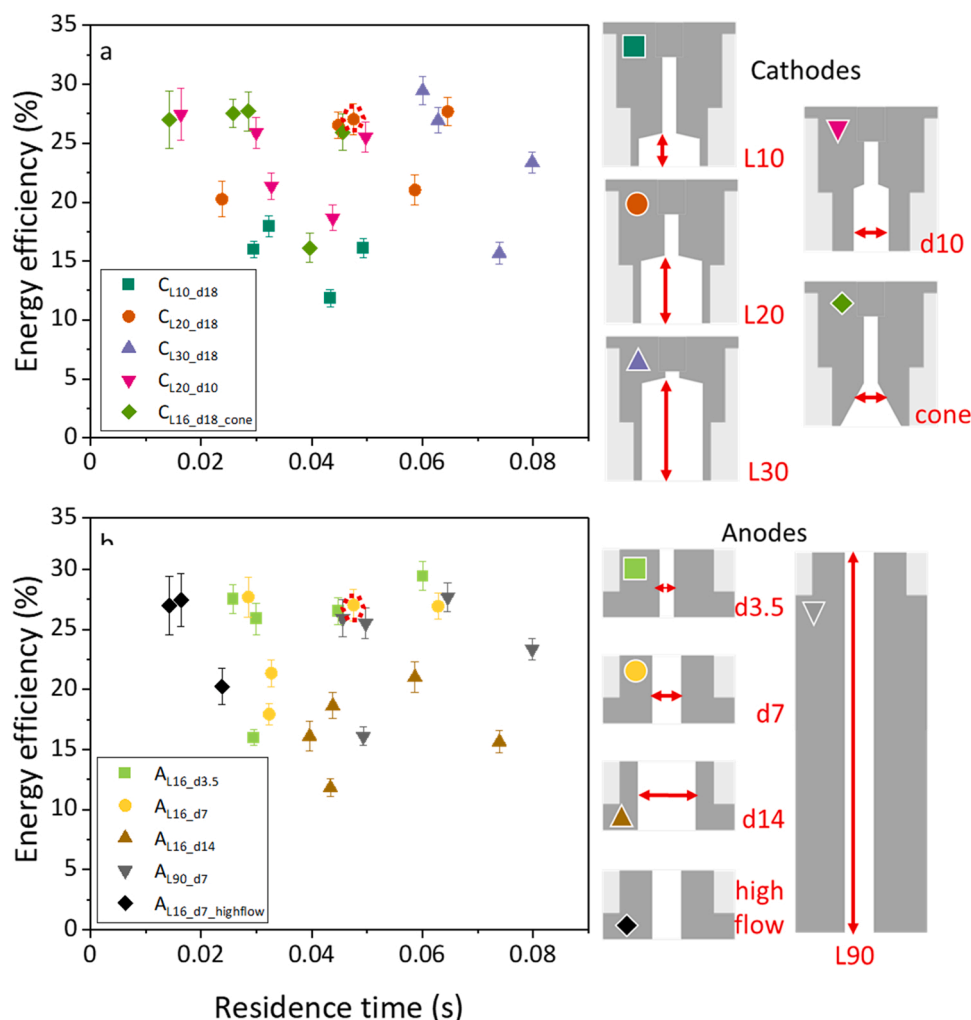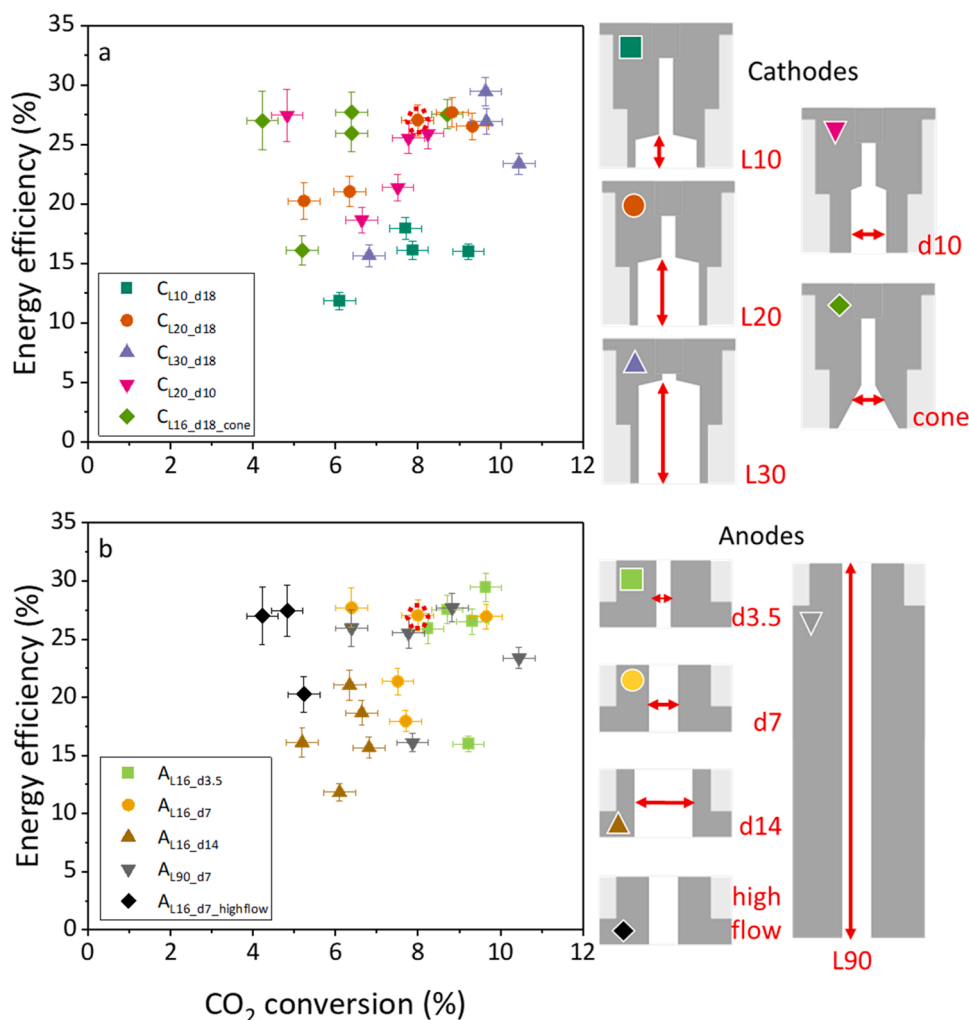
Fig. 13. Energy efficiency as a function of residence time for all electrode combinations (except the inserted anodes): (a) grouped for each cathode and (b) grouped for each anode. The schematic representations are displayed on the right, with a red double arrow to indicate the most important characteristic dimension, also written next to the scheme. The red dotted circle in the graph indicates the basic combination, $C_{L20\_d18}A_{L16\_d7}$.

efficiency, as well as the experimental conditions (i.e. power and flow rate), which are needed to double-check the calculation of the energy efficiency. In addition, some of the literature data in this figure was recalculated to represent coherent values for the conversion and energy efficiency, according to the formulas in the original paper [15]. Indeed, the gas expansion was not always considered for the calculation of the conversion, resulting in overestimated conversions and efficiencies. Secondly, dilution effects should be taken into account when the mixture is diluted with He, Ar or N_2: only the effective conversion is compared in Fig. 15.

In this figure, it is interesting to see that the updated version looks very similar to the original one [15]. Microwave (MW) plasma reactors still achieve the highest energy efficiency, although recent works only obtain these high values when sampling inside or right after the plasma (typically with optical emission spectrometry measurements). Such values are not representative for plasma reactors as part of a process, since the gas will exit the reactor and be subject to recombination reactions, which will lead to a final, lower conversion, well before the gas reaches separation steps. Gliding arc (GA) plasma reactors also perform in the same range as before, with conversions typically below 20 %, in line with our own results. For dielectric barrier discharge (DBD) reactors, some improvements have been demonstrated to reach either higher conversions (exceptionally up to 75 %) or energy efficiencies

(above 20 %), but not the combination of both. Since the publication of the original figure [15], other types of plasma sources have also been investigated more, like atmospheric pressure glow discharges (APGDs) and nanosecond pulsed discharges (NPDs). They display relatively high energy efficiencies (up to 37 %) and achieve higher conversions than e.g. gliding arc reactors (typically up to 30 %). In addition, various experiments have been performed with a carbon bed placed after the plasma reactor, for thermal arc [134,135], GA [45,133,137], and MW [136]. This combination achieves promising conversions (up to 47 %) at reasonable energy efficiencies (up to 56 %). Furthermore, we can consider that the target for efficiency should be lower in these examples, since the separation costs are reduced significantly when all oxygen is removed in such a bed [45].

Despite these recent advances, Fig. 15 looks generally the same as the original figure [15]. No novel plasma research has been able to obtain higher conversions and higher energy efficiencies simultaneously in pure CO_2. This also puts the GAP reactor of our work in perspective: with all the different electrode configurations, it still yields a maximum CO_2 conversion of 10 % at a maximum energy efficiency of 30 %, indicating that this reactor is not the best plasma reactor available in literature. However, its operation at atmospheric pressure still makes it appealing for industrial application. In addition, we believe that further performance improvements are possible, by focusing on the post-plasma zone,

Fig. 14. Performance of all electrode combinations (except the inserted anodes), shown by energy efficiency as a function of CO_2 conversion: (a) grouped for each cathode and (b) grouped for each anode. The schematic representations are displayed on the right, with a red double arrow to indicate the most important characteristic dimension, also written next to the scheme. The red dotted circle in the graph indicates the basic combination, $C_{L20\_d18}A_{L16\_d7}$.

e.g., by nozzles or post-plasma carbon bed or catalysis.

This brief discussion on the results of other plasma reactors (in Fig. 15) is not a comprehensive review, and we refer to other works on the topic [15,54,152]. In the next section, we will discuss how to obtain better performance than in the warm plasma type studied in this work (see Section 5.1 where the conversion is limited to 10 % and the energy efficiency to 30 %). We will elaborate on different plasma types in Section 5.2.1, before we discuss more general improvement strategies in Section 5.2.2.

5.2.1. Different plasmas

DBD reactors apply cold plasma for CO_2 conversion. They have a higher reduced electric field (i.e., ratio of electric field over gas number density), such that electron impact dissociation contributes more [15], which results in a very different plasma chemistry compared to warmer plasmas where thermal chemistry plays a significant role, due to vibrational excitation and subsequent vibrational-translational relaxation [51]. DBD reactors have a simple design and are already applied on large scales for ozone production [10]. High CO_2 conversions are possible, up to 60 % in a DBD operating at 45 W with an inter-electrode distance of 455 μm [114], but the SEI is much higher, i.e., in the range of 36–900 kJ/L. As a result, the energy efficiency in a DBD reactor is typically very low (below 15 %) [15]. Ozkan et al. [107] gave a comprehensive overview of improved CO_2 splitting in a DBD reactor.

Decreasing the operating frequency (from 28.6 kHz to 16.2 kHz) or increasing the barrier thickness (from 2 to 2.8 mm) gives a higher conversion and energy efficiency. The best results were obtained by decreasing the duty cycle from 100 % to 50 % (from pure AC to the burst regime), resulting in a conversion of 26 % for an energy efficiency of 23 %.

Low-pressure plasma reactors achieve better CO_2 conversion and/or energy efficiency, especially in MW plasmas. Record values of 80 % energy efficiency and 25 % CO_2 conversion were obtained in early studies in a MW reactor under subsonic flow conditions [153] and 90 % energy efficiency with supersonic flow [154]. However, these values have not been reproduced since then. A maximum energy efficiency of 47 % was reported by Bongers et al. [58] for a CO_2 conversion of 10 % at 200 mbar. Their maximum CO_2 conversion was 83 %, albeit for a lower energy efficiency of 24 %. These results are very promising, but operating at reduced pressure is challenging even on lab scale, while the cost of the vacuum pump is often not included in the energy efficiency calculations. Efforts to study MW reactors at atmospheric pressure give consistently lower conversions [57,70,76]. Belov et al. [57] reported a drop in CO_2 conversion from 40 % at 0.2 bar to 10 % at 1 bar, which is comparable to the values displayed in Table 3 for other warm plasmas. Similar results were found by Wiegers et al. [76] who reached 8 % as the highest conversion for an energy efficiency of about 18 %. The highest energy efficiency of 50 % was obtained by Mitsingas et al. [70], although

Table 3

Overview of previous work from our lab in warm plasma reactors for CO_2 conversion.

	Basic GAP	Alternative GAP designs	Confined APGD	DVP	RGA
Flow rate (L_s min^{-1})	10–20	10	1–3	5–15	2–8
Power (W)	450–650	500–1100	100–160	450	150–250
SEI (kJ L^{-1})	1–4	1–7	1–6	2–3	1–5
CO_2 conversion (%)	8	4–11	12.5	10	4–8
Energy efficiency (%)	26–31	13–30	24–31	36	36
Reference	[17]	this work	[25]	[24]	[55]

their conversion was again limited to 9 %. Indeed, atmospheric pressure MW plasmas seem to exhibit no better performance than other warm plasmas, such as GA or APGD. Clearly, a lower pressure is beneficial for a high CO_2 conversion, but the costly combination of a MW source with low-pressure system makes it more complex for upscaling than a simpler gliding arc discharge operating at atmospheric pressure [155].

Warm plasmas seem to have reached some limit in conversion and energy efficiency, as we demonstrated in our own experiments in the GAP, which is in line with other warm plasmas from Section 5.1. Moreover, also in MW plasmas, the performance seems to reach the same limits at atmospheric pressure. We believe future efforts should focus on other aspects than the pure reactor design and parameter variation, as discussed with some general strategies next.

5.2.2. Other improvement strategies

First, a co-reactant can be introduced to facilitate the conversion of CO_2. Indeed, the reaction enthalpy of pure CO_2 splitting is high ($\Delta H° = +283$ kJ/mol), but the conversion becomes thermodynamically easier when combined with another compound, such as CH_4 (i.e. dry reforming of methane; $\Delta H° = +247$ kJ/mol) [156]. In addition, reactions with hydrogen carriers can yield liquid products of higher value, such as methanol, which circumvents the energy-intensive processing of syngas and relaxes to some extent the required target for energy efficiency [15]. The CO_2 conversion in the GAP increases from 7.5 % to 24 % upon addition of CH_4 for a much higher energy efficiency of 67 % [18]. Many other co-reactants have been tested, such as O_2, H_2, H_2O, N_2, … among others [19,20,157–160]. The main disadvantage is the challenge to separate the interesting products from the complex output stream, since
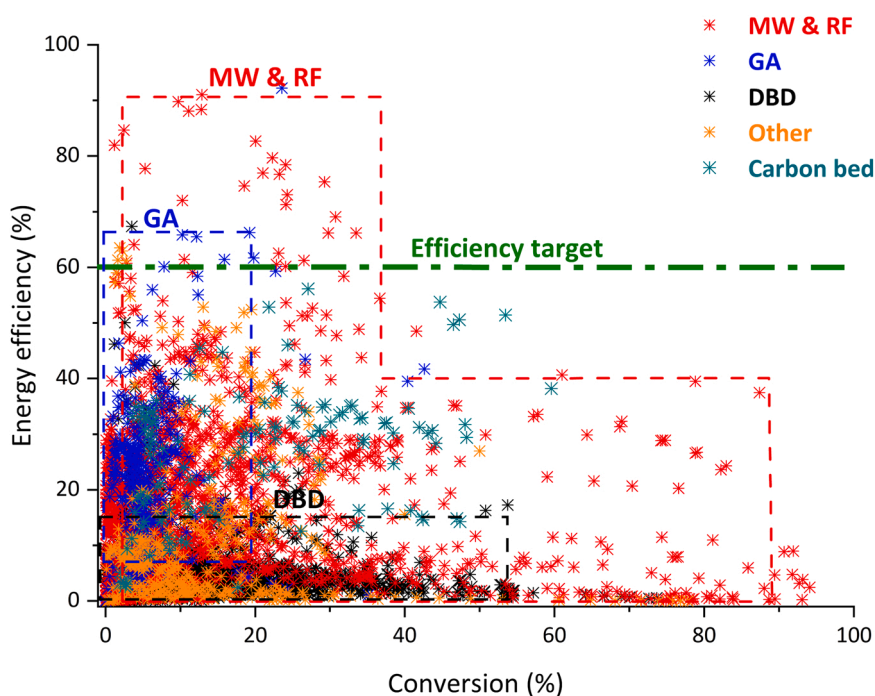
Fig. 15. Comparison of all the data for CO_2 splitting in the various plasma types, showing the energy efficiency as a function of the conversion. Collected from literature by Snoeckx and Bogaerts [15], and updated with additional data points based on more recent literature published since 2016–2017. The efficiency target is defined as the efficiency which should be reached in order to be competitive with other emerging technologies for producing syngas.

plasma is a highly reactive, but non-selective reaction environment. Alternatively, CO_2 is often diluted with a noble gas like argon or helium to obtain a higher conversion, but in this case some energy is inevitably lost to the ionization and excitation of these additional gases [161].

Next, the design of the post-plasma zone could play a more important role than reactor design, especially by introducing a nozzle after a warm plasma. Mercer et al. [37] investigated the effect of a nozzle behind a MW plasma, both experimentally and with CFD simulations, and demonstrated a significant change in the flow geometry, which facilitates fast transport of the produced CO to the exit of the reactor (instead of participating in recombination reactions). Hecimovic et al. [46] managed to increase the CO_2 conversion from 5 % to 35 % in a MW plasma (at 900 mbar) by adding a nozzle in the outlet. They attributed this improved performance to the mixing of the hot plasma gas and the surrounding colder gas, which aligns with other recent insights in MW plasmas [50,51]. Indeed, the conversion is the highest right after the plasma, but drops quickly because CO can recombine with O or O_2 at the high temperatures in the exhaust [48,76]. A nozzle can have a double effect thanks to supersonic expansion: lower pressure in the effluent and reduced temperature, i.e., two effects that can help to reduce recombination losses. More than the reactor design itself, these nozzles seem to hold potential for further improvement for the warm plasmas discussed above, although proper nozzle design is rarely investigated [34].

Besides introducing a nozzle, the addition of (bio)char as a solid reactant after a plasma reactor is perhaps the most successful strategy for improved performance in pure CO_2 conversion [133,134]. Girard-Sahun et al. [45] recently combined such carbon bed with the GAP reactor and obtained almost double the CO_2 conversion. At the same time almost twice the energy efficiency was achieved compared to the same GAP without carbon bed, while removing virtually all O_2 and thus greatly reducing the separation costs. The output CO concentration even increased with a factor three, thanks to the carbon gasification process, resulting in an enhanced CO production. Since the separation costs are the dominant cost factor for plasma-based CO_2 splitting, as demonstrated by van Rooij et al. [56], a carbon bed is a particularly interesting technique to reduce the costs.

The combination of plasma with a catalyst can also help to enhance both conversion and energy efficiency, while tuning the selectivity of the products [54,162]. In fact, simply packing a support material (SiO_2 beads with size of 100–200 μm) without a metal catalyst can increase the CO_2 conversion from 54 % to 74 % in a DBD reactor at 30 W, although the energy efficiency remains low [114]. For the GAP reactor investigated in the current work, the combination with a catalyst is less straightforward. Preliminary tests showed that the catalyst particles are destroyed when placed directly behind the plasma, while placing them further away gives no significant difference. Catalytic materials for oxygen scavenging could also play an important role (in line with the improvements observed for the carbon bed). Delikonstantis et al. [163] recently showed promising results for CO_2 conversion with plasma-assisted chemical looping. The CO_2 conversion was maximum 12 % in their plasma system, but this increased to ca. 29 % by putting an oxygen scavenger in the post-plasma zone. More specifically, they applied the nanostructured CeO_2/Fe_2O_3 material, pre-reduced by H_2 plasma, which could capture the produced oxygen species and suppress CO/O recombination. Their bulk gas temperature was only 773 K, while chemical equilibrium calculations indicate that such high conversion values can only be achieved at temperatures above 2775 K. Their results demonstrate that plasma with post-plasma scavenging materials could significantly overcome chemical equilibrium limits. Plasma catalysis is a growing field on its own, but much more research is needed to understand the underlying mechanisms and improve the performance.

Instead of focusing only on the plasma reactor (and its combination with nozzles, carbon or catalyst bed), one can investigate the overall process design as well, which is often neglected in plasma research. Indeed, our previous work [52] demonstrated a threefold increase in CO_2 conversion when placing plasma reactors in series, from 8 % in the single reactor to 30 % in stage ten. When removing O_2 in between the stages, the conversion improved even more. These results highlight the potential gain from proper process design. A more detailed example of process design is the recent work by Delikonstantis et al. [164] They investigated the process for plasma-assisted ethylene production from methane in a nanosecond pulsed discharge (NPD). They concluded that the plasma process could become economically viable if the electricity prices drop below 50 USD/MWh. Furthermore, the plasma reactor was the dominant cost driver in their process since it consumes ~75 % of the total electric power. However, as mentioned above, Van Rooij et al. [56] found the opposite for CO_2 splitting in a MW reactor: the separation cost was more important. This indicates that both the chemical reaction (CO_2 splitting or methane reforming) and plasma reactor (MW reactor or NPD) play an important role for process design and detailed case studies are needed.

Finally, we briefly mention a few more improvement strategies of sources that are also included in Fig. 15. Pulsing the plasma power is gaining increasing interest for improving the energy efficiency [74,151,165]. Cooling of the electrodes is routinely applied for thermal torches, but can also lead to an improved performance for CO_2 conversion in other plasma types, although the extra energy for cooling is not always taken into account [101]. Even the Sun can be exploited for improvement, although the overall performance is lower than the results discussed in this work [166].

We can conclude that each plasma type and improvement strategy has advantages and disadvantages. On the road to industrial application, pilot-scale demonstrations will have to point out the challenges for upscaling and which technologies might be fit for specific markets. This helps any emerging technology to gain confidence and improve to reach a commercial scale [167], although high-risk investments in development and innovation are crucial to enable these large-scale tests [168]. Considering the urgent need for climate change mitigation, it is time for further development beyond the lab. Only then can we obtain detailed insights in pilot-scale processes and assess possible industrial implementation. Some companies [169–173] are starting to apply plasma technology for sustainable chemistry applications, such as CO_2 conversion and N_2 fixation, but many more initiatives will be needed to address the scale of climate change. From our experiments in this work, we cannot yet draw conclusions on the feasibility of this electrified process at industrial scale, nor on the environmental benefit. For the former, a techno-economic assessment could give a more accurate estimation of the costs. For the latter, a life cycle assessment would be interesting, to investigate the real carbon footprint of the process. This will be the subject of future work.

6. Conclusion

In this work, we evaluated several new electrode configurations in a gliding arc plasmatron (GAP) reactor for CO_2 conversion. The reactor design significantly influences the performance: we obtained the best results with the longest cathode (C_{L30_d18}) and the smallest anode diameter ($A_{L16\_d3.5}$). However, the maximum achieved CO_2 conversion of 10 % is only slightly higher than the 8.6 % obtained in previous work with the basic GAP design [17], while the energy efficiency is comparable, i.e. 30 %. Furthermore, many electrode designs were even detrimental for the performance. A smaller cathode diameter or inserted anodes reduce the conversion, indicating that they suffer from heat losses to the walls, and also that the interaction between the warm plasma core and the surrounding cool edge plays an important role for good performance. A longer anode needs time to warm up and results in a higher conversion, but the energy efficiency is lower, again due to heating losses.

Overall, we observed that the effect of electrode design on the performance is very complex, due to the complicated and strongly coupled gas flow dynamics and plasma behavior (e.g., arc reignition and plasma stability). For this reason, there is not one simple parameter that defines

the optimal design. The anode diameter seems to be the only design parameter with a large effect, confirming previous work and indicating that we probably have reached the limits within the current plasma reactor. The mechanisms underlying our results can be further elucidated with a fluid dynamics model, which will be subject of future work.

Moreover, we compared the performance of our different GAP reactor designs with three other reactors operating in a similar plasma type, i.e. warm plasma reactors at atmospheric pressure and with contact between the plasma and the electrodes. Despite the significant difference in reactor designs, the performance of these warm plasmas is surprisingly similar: they all yield a conversion around 10 % for an energy efficiency around 30 %. These results seem to indicate that the performance limit we encountered in our work is not only present for the GAP reactor, but also for other reactors operating at similar warm plasma conditions, independent of the design. Other plasmas can reach a higher conversion, such as low-pressure MW plasmas and cold DBD reactors, but they have their own challenges, such as vacuum operation and low energy efficiency, respectively. Various improvement strategies are possible, including design of the post-plasma zone with nozzles (to avoid recombination after the plasma) and the combination with a post-plasma carbon bed (again to avoid recombination by removing the O_2 from the mixture and to enhance CO production).

In conclusion, our results indicate that reactor design should not be the only aspect to focus on, and may even have reached its limits once the CO_2 conversion reaches a certain value, i.e., about 10 % in this work. We believe that detailed process design optimisation and pilot-scale demonstrations are a crucial next step to indicate which plasma technologies are fit for specific markets. In future work, we will perform a techno-economic assessment and life cycle analysis to bridge the gap between our lab scale experiments and industrial investments. We believe plasma technology could be a part in the CCU landscape, but it will certainly not be the only one. We will need every initiative today, for the transition to a more sustainable tomorrow.

CRediT authorship contribution statement

Rani Vertongen: Conceptualization, Formal analysis, Investigation, Methodology, Validation, Visualization, Writing – original draft, Writing – review & editing. **Annemie Bogaerts**: Funding acquisition, Project administration, Supervision, Writing – review & editing.

Declaration of Competing Interest

The authors declare the following financial interests/personal relationships which may be considered as potential competing interests: Rani Vertongen reports financial support was provided by Research Foundation Flanders. Annemie Bogaerts reports financial support was provided by European Research Council.

Data availability

Data will be made available on request.

Acknowledgments

Appendix A. Supporting information

Supplementary data associated with this article can be found in the online version at doi:10.1016/j.jcou.2023.102510.

References

[1] IPPC, Climate Change 2022: Impacts, Adaptation and Vulnerability. Contribution of Working Group II to the Sixth Assessment Report of the Intergovernmental Panel on Climate Change, Rep. Clim. Change 1 (2022) 3056. https://www.ipcc.ch/report/ar5/wg3/.

[2] M.V. Deal, W. Evers, G. Vekemans, M. Bulut. CO2 capture and utilization (CCU) matters, 2022. ⟨https://vito.be/sites/vito.be/files/vito_ccu_position_paper.pdf⟩.

[3] S. Valluri, V. Claremboux, S. Kawatra, Opportunities and challenges in CO_2 utilization, J. Environ. Sci. 113 (2022) 322–344, https://doi.org/10.1016/j.jes.2021.05.043.

[4] N. Mac Dowell, P.S. Fennell, N. Shah, G.C. Maitland, The role of CO_2 capture and utilization in mitigating climate change, Nat. Clim. Change 7 (4) (2017) 243–249, https://doi.org/10.1038/nclimate3231.

[5] P. Perreault, N.B. Kummamuru, A.G. Quiroga, S. Lenaerts, CO_2 capture initiatives: are governments, society, industry and the financial sector ready? Curr. Opin. Chem. Eng. 38 (2022), 100874 https://doi.org/10.1016/j.coche.2022.100874.

[6] Po.A. Bruges, Antwerp@C-project. ⟨https://newsroom.portofantwerpbruges.com/het-antwerpc-project-zet-een-belangrijke-volgende-stap-naar-een-halvering-van-de-co2-voetafdruk⟩. (Accessed 15 December 2022).

[7] Porthos. ⟨https://www.porthosco2.nl/⟩. (Accessed 15 December 2022).

[8] C. Hepburn, E. Adlen, J. Beddington, E.A. Carter, S. Fuss, N. Mac Dowell, J. C. Minx, P. Smith, C.K. Williams, The technological and economic prospects for CO_2 utilization and removal, Nature 575 (7781) (2019) 87–97, https://doi.org/10.1038/s41586-019-1681-6.

[9] A.I. Stankiewicz, H. Nigar, Beyond electrolysis: old challenges and new concepts of electricity-driven chemical reactors, React. Chem. Eng. 5 (6) (2020) 1005–1016, https://doi.org/10.1039/D0RE00116C.

[10] E. Delikonstantis, F. Cameli, M. Scapinello, V. Rosa, K.M. Van Geem, G. D. Stefanidis, Low-carbon footprint chemical manufacturing using plasma technology, Curr. Opin. Chem. Eng. 38 (2022), 100857, https://doi.org/10.1016/j.coche.2022.100857.

[11] K.H. Rouwenhorst, Y. Engelmann, K. van't Veer, R.S. Postma, A. Bogaerts, L. Lefferts, Plasma-driven catalysis: green ammonia synthesis with intermittent electricity, Green. Chem. 22 (19) (2020) 6258–6287, https://doi.org/10.1039/D0GC02058C.

[12] K.H. Rouwenhorst, F. Jardali, A. Bogaerts, L. Lefferts, From the Birkeland–Eyde process towards energy-efficient plasma-based NO X synthesis: a techno-economic analysis, Energy Environ. Sci. 14 (5) (2021) 2520–2534, https://doi.org/10.1039/D0EE03763J.

[13] F. Jardali, S. Van Alphen, J. Creel, H.A. Eshtehardi, M. Axelsson, R. Ingels, R. Snyders, A. Bogaerts, NO x production in a rotating gliding arc plasma: Potential avenue for sustainable nitrogen fixation, Green. Chem. 23 (4) (2021) 1748–1757, https://doi.org/10.1039/D0GC03521A.

[14] S. Kelly, A. Bogaerts, Nitrogen fixation in an electrode-free microwave plasma, Joule 5 (11) (2021) 3006–3030, https://doi.org/10.1016/j.joule.2021.09.009.

[15] R. Snoeckx, A. Bogaerts, Plasma technology - a novel solution for CO_2 conversion? Chem. Soc. Rev. 46 (19) (2017) 5805–5863, https://doi.org/10.1039/c6cs00066e.

[16] T. Nunnally, K. Gutsol, A. Rabinovich, A. Fridman, A. Gutsol, A. Kemoun, Dissociation of CO2in a low current gliding arc plasmatron, J. Phys. D: Appl. Phys. 44 (27) (2011), 274009, https://doi.org/10.1088/0022-3727/44/27/274009.

[17] M. Ramakers, G. Trenchev, S. Heijkers, W. Wang, A. Bogaerts, Gliding arc plasmatron: providing an alternative method for carbon dioxide conversion, ChemSusChem 10 (12) (2017) 2642–2652, https://doi.org/10.1002/cssc.201700589.

[18] E. Cleiren, S. Heijkers, M. Ramakers, A. Bogaerts, Dry reforming of methane in a gliding arc plasmatron: towards a better understanding of the plasma chemistry, ChemSusChem 10 (20) (2017) 4025–4036, https://doi.org/10.1002/cssc.201701274.

[19] J. Slaets, M. Aghaei, S. Ceulemans, S. Van Alphen, A. Bogaerts, CO_2 and CH4 conversion in "real" gas mixtures in a gliding arc plasmatron: how do N2 and O2 affect the performance? Green. Chem. 22 (4) (2020) 1366–1377, https://doi.org/10.1039/c9gc03743h.

[20] M. Ramakers, S. Heijkers, T. Tytgat, S. Lenaerts, A. Bogaerts, Combining CO_2 conversion and N2 fixation in a gliding arc plasmatron, J. CO_2 Util. 33 (2019) 121–130, https://doi.org/10.1016/j.jcou.2019.05.015.

[21] E. Vervloessem, M. Aghaei, F. Jardali, N. Hafezkhiabani, A. Bogaerts, Plasma-based N2 fixation into NOx: insights from modeling toward optimum yields and energy costs in a gliding arc plasmatron, ACS Sustain. Chem. Eng. 8 (26) (2020) 9711–9720, https://doi.org/10.1021/acssuschemeng.0c01815.

[22] N. Lu, D. Sun, Y. Xia, K. Shang, B. Wang, N. Jiang, J. Li, Y. Wu, Dry reforming of CH4CO2 in AC rotating gliding arc discharge: effect of electrode structure and gas parameters, Int. J. Hydrog. Energy 43 (29) (2018) 13098–13109, https://doi.org/10.1016/j.ijhydene.2018.05.053.

[23] X. Guofeng, D. Xinwei, Optimization geometries of a vortex gliding-arc reactor for partial oxidation of methane, Energy 47 (1) (2012) 333–339, https://doi.org/10.1016/j.energy.2012.09.032.

[24] G. Trenchev, A. Bogaerts, Dual-vortex plasmatron: a novel plasma source for CO2 conversion, J. CO2 Util. 39 (2020) 101152, https://doi.org/10.1016/j.jcou.2020.03.002.

[25] G. Trenchev, A. Nikiforov, W. Wang, S. Kolev, A. Bogaerts, Atmospheric pressure glow discharge for CO2 conversion: model-based exploration of the optimum reactor configuration, Chem. Eng. J. 362 (2019) 830–841, https://doi.org/10.1016/j.cej.2019.01.091.

[26] Y. Uytdenhouwen, J. Hereijgers, T. Breugelmans, P. Cool, A. Bogaerts, How gas flow design can influence the performance of a DBD plasma reactor for dry reforming of methane, Chem. Eng. J. 405 (2021), 126618, https://doi.org/10.1016/j.cej.2020.126618.

[27] S. Zhang, Y. Gao, H. Sun, Z. Fan, T. Shao, Dry reforming of methane by microsecond pulsed dielectric barrier discharge plasma: optimizing the reactor structures, High. Volt. 7 (4) (2022) 718–729, https://doi.org/10.1049/hve2.12201.

[28] V. Ivanov, T. Paunska, S. Lazarova, A. Bogaerts, S. Kolev, Gliding arc/glow discharge for CO2 conversion: comparing the performance of different discharge configurations, J. CO2 Util. 67 (2023), 102300, https://doi.org/10.1016/j.jcou.2022.102300.

[29] J.-B. Liu, X.-S. Li, J.-L. Liu, A.-M. Zhu, Understanding arc behaviors and achieving the optimal mode in a magnetically-driven gliding arc plasma, Plasma Sources Sci. Technol. 29 (1) (2020), 015022, https://doi.org/10.1088/1361-6595/ab5f1c.

[30] A. Cunha, R. Ribeiro, V. Ribeiro, C. Zucolotto, M. Cevolani, M. Schettino, E. Khalifa, E. Marchiori, A. Labanca, F. Emmerich, Increased arc length and stability in a magnetic gliding arc discharge using a cylindrical notched cathode, Plasma Sources Sci. Technol. 29 (5) (2020), 055008, https://doi.org/10.1088/1361-6595/ab876f.

[31] L. Li, H. Zhang, X. Li, X. Kong, R. Xu, K. Tay, X. Tu, Plasma-assisted CO2 conversion in a gliding arc discharge: Improving performance by optimizing the reactor design, J. CO2 Util. 29 (2019) 296–303, https://doi.org/10.1016/j.jcou.2018.12.019.

[32] D.H. Lee, K.-T. Kim, H.S. Kang, S. Jo, Y.-H. Song, Optimization of NH3 decomposition by control of discharge mode in a rotating arc, Plasma Chem. Plasma Process. 34 (1) (2014) 111–124, https://doi.org/10.1007/s11090-013-9495-z.

[33] A. Czernichowski, M. Czernichowski, Further development of plasma sources: the GlidArc-III, 17th Int. Symp. plasma Chem. Toronto, Canada, Citeseer, 2005, pp. 1–4.

[34] M. Khaji, K. Peerenboom, J. van der Mullen, G. Degrez, 2D numerical modeling for plasma-assisted CO2 pooling in supersonic nozzles: importance of a proper nozzle contour design, J. Phys. D: Appl. Phys. 54 (16) (2021), 165202, https://doi.org/10.1088/1361-6463/abd355.

[35] D.K. Dinh, G. Trenchev, D.H. Lee, A. Bogaerts, Arc plasma reactor modification for enhancing performance of dry reforming of methane, J. CO2 Util. 42 (2020), 101352, https://doi.org/10.1016/j.jcou.2020.101352.

[36] S. Van Alphen, H. Ahmadi Eshtehardi, C. O'Modhrain, J. Bogaerts, H. Van Poyer, J. Creel, M.-P. Delplancke, R. Snyders, A. Bogaerts, Effusion nozzle for energy-efficient NOx production in a rotating gliding arc plasma reactor, Chem. Eng. J. 443 (2022), 136529, https://doi.org/10.1016/j.cej.2022.136529.

[37] E.R. Mercer, S. Van Alphen, C.F.A.M. van Deursen, T.W.H. Righart, W.A. Bongers, R. Snyders, A. Bogaerts, M.C.M. van de Sanden, F.J.J. Peeters, Post-plasma quenching to improve conversion and energy efficiency in a CO2 microwave plasma, Fuel 334 (2023), 126734, https://doi.org/10.1016/j.fuel.2022.126734.

[38] B. Raja, R. Sarathi, R. Vinu, Development of a Swirl-Induced Rotating Glow Discharge Reactor for CO2 Conversion: Fluid Dynamics and Discharge Dynamics Studies, Energy Technol. 8 (12) (2020), 2000535, https://doi.org/10.1002/ente.202000535.

[39] X. Pei, D. Gidon, D.B. Graves, Propeller arc: design and basic characteristics, Plasma Sources Sci. Technol. 27 (12) (2018), 125007, https://doi.org/10.1088/1361-6595/aaf7ef.

[40] G. Trenchev, S. Kolev, W. Wang, M. Ramakers, A. Bogaerts, CO2 conversion in a gliding arc plasmatron: multidimensional modeling for improved efficiency, J. Phys. Chem. C 121 (44) (2017) 24470–24479, https://doi.org/10.1021/acs.jpcc.7b08511.

[41] M. Ramakers, J.A. Medrano, G. Trenchev, F. Gallucci, A. Bogaerts, Revealing the arc dynamics in a gliding arc plasmatron: a better insight to improve CO2 conversion, Plasma Sources Sci. Technol. 26 (12) (2017), https://doi.org/10.1088/1361-6595/aa9531.

[42] S. Gröger, M. Ramakers, M. Hamme, J.A. Medrano, N. Bibinov, F. Gallucci, A. Bogaerts, P. Awakowicz, Characterization of a nitrogen gliding arc plasmatron using optical emission spectroscopy and high-speed camera, J. Phys. D: Appl. Phys. 52 (6) (2019), https://doi.org/10.1088/1361-6463/aaefe4.

[43] S.-Y. Zhang, X.-S. Li, H.-P. Li, J.-L. Liu, A.-M. Zhu, Caudal autotomy and regeneration of arc in a 3D gliding arc discharge plasma, J. Phys. D: Appl. Phys. 54 (30) (2021), 305203, https://doi.org/10.1088/1361-6463/abfe3a.

[44] S. Xu, F. Song, X. Yang, Y. Zhong, Y. Gao, Experimental study on the influence of an extension tube on the evolution process and characteristic parameters of a gliding arc, Appl. Sci. 9 (7) (2019) 1347, https://doi.org/10.3390/app9071347.

[45] F. Girard-Sahun, O. Biondo, G. Trenchev, G.J. van Rooij, A. Bogaerts, Carbon bed post-plasma to enhance the CO2 conversion and remove O2 from the product stream, Chem. Eng. J. 442 (2022), 136268, https://doi.org/10.1016/j.cej.2022.136268.

[46] A. Hecimovic, F.A. D'Isa, E. Carbone, U. Fantz, Enhancement of CO2 conversion in microwave plasmas using a nozzle in the effluent, J. CO2 Util. 57 (2022), 101870, https://doi.org/10.1016/j.jcou.2021.101870.

[47] S. Van Alphen, A. Hecimovic, C.K. Kiefer, U. Fantz, R. Snyders, A. Bogaerts, Modelling post-plasma quenching nozzles for improving the performance of CO2 microwave plasmas, Chem. Eng. J. 462 (2023), 142217, https://doi.org/10.1016/j.cej.2023.142217.

[48] V. Vermeiren, A. Bogaerts, Plasma-based CO2 conversion: to quench or not to quench? J. Phys. Chem. C 124 (34) (2020) 18401–18415, https://doi.org/10.1021/acs.jpcc.0c04257.

[49] C.S. Kalra, Y.I. Cho, A. Gutsol, A. Fridman, T.S. Rufael, Gliding arc in tornado using a reverse vortex flow, Rev. Sci. Instrum. 76 (2) (2005), https://doi.org/10.1063/1.1854215.

[50] D.C.M. van den Bekerom, J.M.P. Linares, T. Verreycken, E.M. van Veldhuizen, S. Nijdam, G. Berden, W.A. Bongers, M.C.M. van de Sanden, G.J. van Rooij, The importance of thermal dissociation in CO2 microwave discharges investigated by power pulsing and rotational Raman scattering, Plasma Sources Sci. Technol. 28 (5) (2019), 055015, https://doi.org/10.1088/1361-6595/aaf519.

[51] A. van de Steeg, P. Viegas, A. Silva, T. Butterworth, A. van Bavel, J. Smits, P. Diomede, M. van de Sanden, G. van Rooij, Redefining the microwave plasma-mediated CO2 reduction efficiency limit: the role of O–CO2 association, ACS Energy Lett. 6 (8) (2021) 2876–2881, https://doi.org/10.1021/acsenergylett.1c01206.

[52] R. Vertongen, G. Trenchev, R. Van Loenhout, A. Bogaerts, Enhancing CO2 conversion with plasma reactors in series and O2 removal, J. CO2 Util. 66 (2022), 102252, https://doi.org/10.1016/j.jcou.2022.102252.

[53] G. Komarzyniec, M. Aftyka, Operating problems of arc plasma reactors powered by AC/DC/AC converters, Appl. Sci. 10 (9) (2020) 3295, https://doi.org/10.3390/app10093295.

[54] G. Chen, R. Snyders, N. Britun, CO2 conversion using catalyst-free and catalyst-assisted plasma-processes: recent progress and understanding, J. CO2 Util. 49 (2021), 101557, https://doi.org/10.1016/j.jcou.2021.101557.

[55] S. Stollenwerk, CO2 and CH4 conversion in a novel rotating gliding arc, M.Sc. Thesis, (c:lvd:14941049) (2019).

[56] G.J. van Rooij, H.N. Akse, W.A. Bongers, M.C.M. van de Sanden, Plasma for electrification of chemical industry: a case study on CO2reduction, Plasma Phys. Control. Fusion 60 (1) (2018), https://doi.org/10.1088/1361-6587/aa8f7d.

[57] I. Belov, V. Vermeiren, S. Paulussen, A. Bogaerts, Carbon dioxide dissociation in a microwave plasma reactor operating in a wide pressure range and different gas inlet configurations, J. CO2 Util. 24 (2018) 386–397, https://doi.org/10.1016/j.jcou.2017.12.009.

[58] W. Bongers, H. Bouwmeester, B. Wolf, F. Peeters, S. Welzel, D. van den Bekerom, N. den Harder, A. Goede, M. Graswinckel, P.W. Groen, Plasma-driven dissociation of CO2 for fuel synthesis, Plasma Process. Polym. 14 (6) (2017), 1600126, https://doi.org/10.1002/ppap.201600126.

[59] N. Britun, T. Godfroid, R. Snyders, Insights into CO2 conversion in pulsed microwave plasma using optical spectroscopy, J. CO2 Util. 41 (2020) 101239, https://doi.org/10.1016/j.jcou.2020.101239.

[60] N. Britun, T. Silva, G. Chen, T. Godfroid, J. van der Mullen, R. Snyders, Plasma-assisted CO2 conversion: optimizing performance via microwave power modulation, J. Phys. D: Appl. Phys. 51 (14) (2018), 144002, https://doi.org/10.1088/1361-6463/aab1ad.

[61] F. D'Isa, E. Carbone, A. Hecimovic, U. Fantz, Performance analysis of a 2.45 GHz microwave plasma torch for CO2 decomposition in gas swirl configuration, Plasma Sources Sci. Technol. 29 (10) (2020), 105009, https://doi.org/10.1088/1361-6595/abaa84.

[62] N. den Harder, D.C. van den Bekerom, R.S. Al, M.F. Graswinckel, J.M. Palomares, F.J. Peeters, S. Ponduri, T. Minea, W.A. Bongers, M.C. van de Sanden, Homogeneous CO2 conversion by microwave plasma: wave propagation and diagnostics, Plasma Process. Polym. 14 (6) (2017), 1600120, https://doi.org/10.1002/ppap.201600120.

[63] E.J. Devid, M. Ronda-Lloret, D. Zhang, E. Schuler, D. Wang, C.H. Liang, Q. Huang, G. Rothenberg, N.R. Shiju, A.W. Kleyn, Enhancing CO2 plasma conversion using metal grid catalysts, J. Appl. Phys. 129 (5) (2021), https://doi.org/10.1063/5.0033212.

[64] C. Guoxing, B. Nikolay, G. Thomas, D.O. Marie-Paule, S. Rony, Role of Plasma Catalysis in the Microwave Plasma-Assisted Conversion of CO2, in: K. Iyad, S. Hassan (Eds.), Green Chemical, IntechOpen, Rijeka, 2017, https://doi.org/10.5772/67874.

[65] C. Harvey, S. Vandenburg, A.R. Ellingboe, A non-equilibrium atmospheric pressure Capacitively-Coupled-Plasma (CCP) driven at VHF (162 MHz) for plasma catalysis of CO2 into CO, Curr. Appl. Phys. 28 (2021) 45–51, https://doi.org/10.1016/j.cap.2021.04.016.

[66] A. Hecimovic, F. D'Isa, E. Carbone, A. Drenik, U. Fantz, Quantitative gas composition analysis method for a wide pressure range up to atmospheric pressure—CO2 plasma case study, Rev. Sci. Instrum. 91 (11) (2020), 113501, https://doi.org/10.1063/5.0013413.

[67] Q. Huang, D. Zhang, D. Wang, K. Liu, A.W. Kleyn, Carbon dioxide dissociation in non-thermal radiofrequency and microwave plasma, J. Phys. D: Appl. Phys. 50 (29) (2017), 294001, https://doi.org/10.1088/1361-6463/aa754e.

[68] H. Kim, S. Song, C.P. Tom, F. Xie, Carbon dioxide conversion in an atmospheric pressure microwave plasma reactor: Improving efficiencies by enhancing afterglow quenching, J. CO2 Util. 37 (2020) 240–247, https://doi.org/10.1016/j.jcou.2019.12.011.

[69] D. Mansfeld, S. Sintsov, N. Chekmarev, A. Vodopyanov, Conversion of carbon dioxide in microwave plasma torch sustained by gyrotron radiation at frequency

of 24 GHz at atmospheric pressure, J. CO2 Util. 40 (2020), 101197, https://doi.org/10.1016/j.jcou.2020.101197.

[70] C.M. Mitsingas, R. Rajasegar, S. Hammack, H. Do, T. Lee, High energy efficiency plasma conversion of CO 2 at atmospheric pressure using a direct-coupled microwave plasma system, IEEE Trans. Plasma Sci. 44 (4) (2016) 651–656, https://doi.org/10.1109/TPS.2016.2531641.

[71] S. Mohsenian, D. Nagassou, S. Bhatta, R. Elahi, J.P. Trelles, Design and characterization of a solar-enhanced microwave plasma reactor for atmospheric pressure carbon dioxide decomposition, Plasma Sources Sci. Technol. 28 (6) (2019), 065001, https://doi.org/10.1088/1361-6595/ab1c43.

[72] S.H. Moreno, A.I. Stankiewicz, G.D. Stefanidis, A two-step modelling approach for plasma reactors – experimental validation for CO2 dissociation in surface wave microwave plasma, React. Chem. Eng. 4 (7) (2019) 1253–1269, https://doi.org/10.1039/C9RE00022D.

[73] Y. Qin, G. Niu, X. Wang, D. Luo, Y. Duan, Conversion of CO2 in a low-powered atmospheric microwave plasma: In-depth study on the trade-off between CO2 conversion and energy efficiency, Chem. Phys. 538 (2020), https://doi.org/10.1016/j.chemphys.2020.110913.

[74] S. Soldatov, E. Carbone, A. Kuhn, G. Link, J. Jelonnek, R. Dittmeyer, A. Navarrete, Efficiency of a compact CO2 coaxial plasma torch driven by ultrafast microwave power pulsing: stability and plasma gas flow dynamics, J. CO2 Util. 58 (2022), 101916, https://doi.org/10.1016/j.jcou.2022.101916.

[75] S. Soldatov, G. Link, L. Silberer, C.M. Schmedt, E. Carbone, F. D'Isa, J. Jelonnek, R. Dittmeyer, A. Navarrete, Time-resolved optical emission spectroscopy reveals nonequilibrium conditions for CO2 splitting in atmospheric plasma sustained with ultrafast microwave pulsation, ACS Energy Lett. 6 (1) (2021) 124–130, https://doi.org/10.1021/acsenergylett.0c01983.

[76] K. Wiegers, A. Schulz, M. Walker, G.E.M. Tovar, Determination of the conversion and efficiency for CO2 in an atmospheric pressure microwave plasma torch, Chem. Ing. Tech. 94 (3) (2022) 299–308, https://doi.org/10.1002/cite.202100149.

[77] A.J. Wolf, F.J.J. Peeters, P.W.C. Groen, W.A. Bongers, M.C.M. van de Sanden, CO2 conversion in nonuniform discharges: disentangling dissociation and recombination mechanisms, J. Phys. Chem. C 124 (31) (2020) 16806–16819, https://doi.org/10.1021/acs.jpcc.0c03637.

[78] R. Yang, D. Zhang, K. Zhu, H. Zhou, X. Ye, A.W. Kleyn, Study of the conversion reaction of CO2 and CO2H2 mixtures in radio frequency discharge plasma, Acta Phys. -Chim. Sin. 35 (3) (2019) 292–298, https://doi.org/10.3866/PKU.WHXB201803121.

[79] D. Zhang, Q. Huang, E.J. Devid, E. Schuler, N.R. Shiju, G. Rothenberg, G. van Rooij, R. Yang, K. Liu, A.W. Kleyn, Tuning of conversion and optical emission by electron temperature in inductively coupled CO2 plasma, J. Phys. Chem. C 122 (34) (2018) 19338–19347, https://doi.org/10.1021/acs.jpcc.8b04716.

[80] L. Li, H. Zhang, X. Li, J. Huang, X. Kong, R. Xu, X. Tu, Magnetically enhanced gliding arc discharge for CO2 activation, J. CO2 Util. 35 (2020) 28–37, https://doi.org/10.1016/j.jcou.2019.08.021.

[81] D. Nagassou, S. Mohsenian, S. Bhatta, R. Elahi, J.P. Trelles, Solar–gliding arc plasma reactor for carbon dioxide decomposition: design and characterization, Sol. Energy 180 (2019) 678–689, https://doi.org/10.1016/j.solener.2019.01.070.

[82] D. Nagassou, S. Mohsenian, M. Nallar, P. Yu, H.-W. Wong, J.P. Trelles, Decomposition of CO2 in a solar-gliding arc plasma reactor: effects of water, nitrogen, methane, and process optimization, J. CO2 Util. 38 (2020) 39–48, https://doi.org/10.1016/j.jcou.2020.01.007.

[83] H. Sun, Z. Chen, J. Chen, H. Long, Y. Wu, W. Zhou, The influence of back-breakdown on the CO2 conversion in gliding arc plasma: based on experiments of different materials and improved structures, J. Phys. D: Appl. Phys. 54 (49) (2021), https://doi.org/10.1088/1361-6463/ac2335.

[84] W. Wang, D. Mei, X. Tu, A. Bogaerts, Gliding arc plasma for CO2 conversion: Better insights by a combined experimental and modelling approach, Chem. Eng. J. 330 (2017) 11–25, https://doi.org/10.1016/j.cej.2017.07.133.

[85] H. Zhang, L. Li, X. Li, W. Wang, J. Yan, X. Tu, Warm plasma activation of CO2 in a rotating gliding arc discharge reactor, J. CO2 Util. 27 (2018) 472–479, https://doi.org/10.1016/j.jcou.2018.08.020.

[86] H. Zhang, L. Li, R. Xu, J. Huang, N. Wang, X. Li, X. Tu, Plasma-enhanced catalytic activation of CO2 in a modified gliding arc reactor, Waste Dispos. Sustain. Energy 2 (2) (2020) 139–150, https://doi.org/10.1007/s42768-020-00034-z.

[87] D. Adrianto, Z. Sheng, T. Nozaki, Mechanistic study on nonthermal plasma conversion of CO2, Int. J. Plasma Environ. Sci. Technol. 14 (e01003) (2020) 9, https://doi.org/10.34343/ijpest.2020.14.e01003.

[88] R. Afriansyah, S. Bismo, S. Nadhifa, Performance test and operating condition optimization of parallel plate plasma reactor for carbon dioxide decomposition, Int. J. Technol. 9 (6) (2018) 291–319, https://doi.org/10.14716/ijtech.v9i6.2363.

[89] B. Ashford, Y. Wang, C.-K. Poh, L. Chen, X. Tu, Plasma-catalytic conversion of CO2 to CO over binary metal oxide catalysts at low temperatures, Appl. Catal. B: Environ. 276 (2020), 119110, https://doi.org/10.1016/j.apcatb.2020.119110.

[90] A.M. Banerjee, J. Billinger, K.J. Nordheden, F.J.J. Peeters, Conversion of CO2 in a packed-bed dielectric barrier discharge reactor, J. Vac. Sci. Technol. A 36 (4) (2018) 04F403, https://doi.org/10.1116/1.5024400.

[91] A. Barkhordari, S. Karimian, A. Rodero, D.A. Krawczyk, S.I. Mirzaei, A. Falahat, Carbon dioxide decomposition by a parallel-plate plasma reactor: experiments and 2-D modelling, Appl. Sci. 11 (21) (2021), https://doi.org/10.3390/app112110047.

[92] P. Chen, J. Shen, T. Ran, T. Yang, Y. Yin, Investigation of operating parameters on CO2 splitting by dielectric barrier discharge plasma, Plasma Sci. Technol. 19 (12) (2017), 125505, https://doi.org/10.1088/2058-6272/aa8903.

[93] W. Ding, M. Xia, C. Shen, Y. Wang, Z. Zhang, X. Tu, C.-j Liu, Enhanced CO2 conversion by frosted dielectric surface with ZrO2 coating in a dielectric barrier discharge reactor, J. CO2 Util. 61 (2022), 102045, https://doi.org/10.1016/j.jcou.2022.102045.

[94] Q. Huang, Z. Liang, F. Qi, N. Zhang, J. Yang, J. Liu, C. Tian, C. Fu, X. Tang, D. Wu, J. Wang, X. Wang, W. Chen, Carbon dioxide conversion synergistically activated by dielectric barrier discharge plasma and the CsPbBr3@TiO2 photocatalyst, J. Phys. Chem. Lett. 13 (10) (2022) 2418–2427, https://doi.org/10.1021/acs.jpclett.2c00253.

[95] M.R. Jahanbakhsh, H. Taghvaei, O. Khalifeh, M. Ghanbari, M.R. Rahimpour, Low-temperature CO2 splitting in a noncatalytic dielectric-barrier discharge plasma: effect of operational parameters with a new strategy of experimentation, Energy Fuels 34 (11) (2020) 14321–14332, https://doi.org/10.1021/acs.energyfuels.0c02116.

[96] H. Ji, L. Lin, K. Chang, Plasma-assisted CO2 decomposition catalyzed by CeO2 of various morphologies, J. CO2 Util. 68 (2023), 102351, https://doi.org/10.1016/j.jcou.2022.102351.

[97] P. Kaliyappan, A. Paulus, J. D'Haen, P. Samyn, Y. Uytdenhouwen, N. Hafezkhiabani, A. Bogaerts, V. Meynen, K. Elen, A. Hardy, M.K. Van Bael, Probing the impact of material properties of core-shell SiO2@TiO2 spheres on the plasma-catalytic CO2 dissociation using a packed bed DBD plasma reactor, J. CO2 Util. 46 (2021), 101468, https://doi.org/10.1016/j.jcou.2021.101468.

[98] A. Li, Y. Pei, X. Tao, Z. Wang, Effects of discharge parameters on carbon dioxide conversion in TiO2 packed dielectric barrier discharge at atmospheric pressure, SN Appl. Sci. 1 (8) (2019) 816, https://doi.org/10.1007/s42452-019-0847-z.

[99] J. Li, X. Zhai, C. Ma, S. Zhu, F. Yu, B. Dai, G. Ge, D. Yang, DBD plasma combined with different foam metal electrodes for CO2 decomposition: experimental results and DFT validations, Nanomaterials 9 (11) (2019) 1595, https://doi.org/10.3390/nano9111595.

[100] J. Li, S. Zhu, K. Lu, C. Ma, D. Yang, F. Yu, CO2 conversion in a coaxial dielectric barrier discharge plasma reactor in the presence of mixed ZrO2-CeO2, J. Environ. Chem. Eng. 9 (1) (2021), 104654, https://doi.org/10.1016/j.jece.2020.104654.

[101] N. Lu, N. Liu, C. Zhang, Y. Su, K. Shang, N. Jiang, J. Li, Y. Wu, CO2 conversion promoted by potassium intercalated g-C3N4 catalyst in DBD plasma system, Chem. Eng. J. 417 (2021), 129283, https://doi.org/10.1016/j.cej.2021.129283.

[102] N. Lu, D. Sun, C. Zhang, N. Jiang, K. Shang, X. Bao, J. Li, Y. Wu, CO2 conversion in non-thermal plasma and plasma/g-C3N4 catalyst hybrid processes, J. Phys. D: Appl. Phys. 51 (9) (2018), 094001, https://doi.org/10.1088/1361-6463/aaa919.

[103] D. Mei, Y.-L. He, S. Liu, J. Yan, X. Tu, Optimization of CO2 conversion in a cylindrical dielectric barrier discharge reactor using design of experiments, Plasma Process. Polym. 13 (5) (2016) 544–556, https://doi.org/10.1002/ppap.201500159.

[104] D. Mei, X. Tu, Atmospheric pressure non-thermal plasma activation of CO2 in a packed-bed dielectric barrier discharge reactor, ChemPhysChem 18 (22) (2017) 3253–3259, https://doi.org/10.1002/cphc.201700752.

[105] P. Navascués, J. Cotrino, A.R. González-Elipe, A. Gómez-Ramírez, Plasma assisted CO2 dissociation in pure and gas mixture streams with a ferroelectric packed-bed reactor in ambient conditions, Chem. Eng. J. 430 (2022), https://doi.org/10.1016/j.cej.2021.133066.

[106] G. Niu, Y. Qin, W. Li, Y. Duan, Investigation of CO2 splitting process under atmospheric pressure using multi-electrode cylindrical DBD plasma reactor, Plasma Chem. Plasma Process. 39 (4) (2019) 809–824, https://doi.org/10.1007/s11090-019-09955-y.

[107] A. Ozkan, A. Bogaerts, F. Reniers, Routes to increase the conversion and the energy efficiency in the splitting of CO2 by a dielectric barrier discharge, J. Phys. D: Appl. Phys. 50 (8) (2017), 084004, https://doi.org/10.1088/1361-6463/aa562c.

[108] J.O. Pou, E. Estopañán, J. Fernandez-Garcia, R. Gonzalez-Olmos, Sustainability assessment of the utilization of CO2 in a dielectric barrier discharge reactor powered by photovoltaic energy, Processes 10 (9) (2022) 1851, https://doi.org/10.3390/pr10091851.

[109] D. Ray, P. Chawdhury, K.V.S.S. Bhargavi, S. Thatikonda, N. Lingaiah, C. Subrahmanyam, Ni and Cu oxide supported γ-Al2O3 packed DBD plasma reactor for CO2 activation, J. CO2 Util. 44 (2021), 101400, https://doi.org/10.1016/j.jcou.2020.101400.

[110] D. Ray, R. Saha, S. Ch, DBD plasma assisted CO2 decomposition: influence of diluent gases, Catalysts 7 (9) (2017) 244, https://doi.org/10.3390/catal7090244.

[111] D. Ray, C. Subrahmanyam, CO2 decomposition in a packed DBD plasma reactor: influence of packing materials, RSC Adv. 6 (45) (2016) 39492–39499, https://doi.org/10.1039/C5RA27085E.

[112] H. Taghvaei, E. Pirzadeh, M. Jahanbakhsh, O. Khalifeh, M.R. Rahimpour, Polyurethane foam: a novel support for metal oxide packing used in the non-thermal plasma decomposition of CO2, J. CO2 Util. 44 (2021), 101398, https://doi.org/10.1016/j.jcou.2020.101398.

[113] M. Umamaheswara Rao, K.V.S.S. Bhargavi, P. Chawdhury, D. Ray, S.R.K. Vanjari, C. Subrahmanyam, Non-thermal plasma assisted CO2 conversion to CO: Influence of non-catalytic glass packing materials, Chem. Eng. Sci. 267 (2023), 118376, https://doi.org/10.1016/j.ces.2022.118376.

[114] Y. Uytdenhouwen, K.M. Bal, I. Michielsen, E.C. Neyts, V. Meynen, P. Cool, A. Bogaerts, How process parameters and packing materials tune chemical equilibrium and kinetics in plasma-based CO2 conversion, Chem. Eng. J. 372 (2019) 1253–1264, https://doi.org/10.1016/j.cej.2019.05.008.

[115] Y. Uytdenhouwen, S. Van Alphen, I. Michielsen, V. Meynen, P. Cool, A. Bogaerts, A packed-bed DBD micro plasma reactor for CO_2 dissociation: does size matter? Chem. Eng. J. 348 (2018) 557–568, https://doi.org/10.1016/j.cej.2018.04.210.

[116] B. Wang, X. Li, X. Wang, B. Zhang, Effect of filling materials on CO_2 conversion with a dielectric barrier discharge reactor, J. Environ. Chem. Eng. 9 (6) (2021), 106370, https://doi.org/10.1016/j.jece.2021.106370.

[117] B. Wang, X. Wang, H. Su, Influence of electrode interval and barrier thickness in the segmented electrode micro-plasma DBD reactor on CO_2 decomposition, Plasma Chem. Plasma Process. 40 (5) (2020) 1189–1206, https://doi.org/10.1007/s11090-020-10091-1.

[118] B. Wang, X. Wang, B. Zhang, Dielectric barrier micro-plasma reactor with segmented outer electrode for decomposition of pure CO_2, Front. Chem. Sci. Eng. 15 (3) (2021) 687–697, https://doi.org/10.1007/s11705-020-1974-1.

[119] L. Wang, X. Du, Y. Yi, H. Wang, M. Gul, Y. Zhu, X. Tu, Plasma-enhanced direct conversion of CO_2 to CO over oxygen-deficient Mo-doped CeO_2, Chem. Commun. 56 (94) (2020) 14801–14804, https://doi.org/10.1039/D0CC06514E.

[120] T. Wang, H. Liu, X. Xiong, X. Feng, Conversion of carbon dioxide to carbon monoxide by pulse dielectric barrier discharge plasma, IOP Conf. Ser.: Earth Environ. Sci. 52 (1) (2017), 012100, https://doi.org/10.1088/1742-6596/52/1/012100.

[121] P. Wu, X. Li, N. Ullah, Z. Li, Synergistic effect of catalyst and plasma on CO_2 decomposition in a dielectric barrier discharge plasma reactor, Mol. Catal. 499 (2021), 111304, https://doi.org/10.1016/j.mcat.2020.111304.

[122] M. Xia, W. Ding, C. Shen, Z. Zhang, C.-j Liu, CeO_2-Enhanced CO_2 decomposition via frosted dielectric barrier discharge plasma, Ind. Eng. Chem. Res. 61 (29) (2022) 10455–10460, https://doi.org/10.1021/acs.iecr.2c00201.

[123] S. Xiaozhen, Z. Yong, Q. Fuyang, W. Xiangrong, Effect of glass additions on Ca0. 8Sr0. 2TiO3 ceramics as dielectrics for a cylindrical dielectric barrier discharge reactor in CO_2 plasma, Rare Met. Mater. Eng. 45 (12) (2016) 3037–3042, https://doi.org/10.1016/S1875-5372(17)30050-4.

[124] S. Xu, P.I. Khalaf, P.A. Martin, J.C. Whitehead, CO_2 dissociation in a packed-bed plasma reactor: effects of operating conditions, Plasma Sources Sci. Technol. 27 (7) (2018), 075009, https://doi.org/10.1088/1361-6595/aacd6a.

[125] S. Xu, J.C. Whitehead, P.A. Martin, CO_2 conversion in a non-thermal, barium titanate packed bed plasma reactor: the effect of dilution by Ar and N2, Chem. Eng. J. 327 (2017) 764–773, https://doi.org/10.1016/j.cej.2017.06.090.

[126] K. Zhang, A.P. Harvey, CO_2 decomposition to CO in the presence of up to 50 % O2 using a non-thermal plasma at atmospheric temperature and pressure, Chem. Eng. J. 405 (2021), https://doi.org/10.1016/j.cej.2020.126625.

[127] K. Zhang, G. Zhang, X. Liu, A.N. Phan, K. Luo, A study on CO_2 decomposition to CO and O2 by the combination of catalysis and dielectric-barrier discharges at low temperatures and ambient pressure, Ind. Eng. Chem. Res. 56 (12) (2017) 3204–3216, https://doi.org/10.1021/acs.iecr.6b04570.

[128] A. Zhou, D. Chen, B. Dai, C. Ma, P. Li, F. Yu, Direct decomposition of CO_2 using self-cooling dielectric barrier discharge plasma, Greenh. Gases: Sci. Technol. 7 (4) (2017) 721–730, https://doi.org/10.1002/ghg.1683.

[129] A. Zhou, D. Chen, C. Ma, F. Yu, B. Dai, DBD Plasma-ZrO2 catalytic decomposition of CO_2 at low temperatures, Catalysts 8 (7) (2018), https://doi.org/10.3390/catal8070256.

[130] M. Zhu, S. Hu, F. Wu, H. Ma, S. Xie, C. Zhang, CO_2 dissociation in a packed bed DBD reactor: effect of streamer discharge, J. Phys. D: Appl. Phys. 55 (22) (2022), 225207, https://doi.org/10.1088/1361-6463/ac55c1.

[131] S. Zhu, A. Zhou, F. Yu, B. Dai, C. Ma, Enhanced CO_2 decomposition via metallic foamed electrode packed in self-cooling DBD plasma device, Plasma Sci. Technol. 21 (8) (2019), 085504, https://doi.org/10.1088/2058-6272/ab15e5.

[132] R. Hosseini Rad, V. Brüser, M. Schiorlin, J. Schäfer, R. Brandenburg, Enhancement of CO_2 splitting in a coaxial dielectric barrier discharge by pressure increase, packed bed and catalyst addition, Chem. Eng. J. 456 (2023), 141072, https://doi.org/10.1016/j.cej.2022.141072.

[133] J. Huang, H. Zhang, Q. Tan, L. Li, R. Xu, Z. Xu, X. Li, Enhanced conversion of CO_2 into O2-free fuel gas via the Boudouard reaction with biochar in an atmospheric plasmatron, J. CO_2 Util. 45 (2021), https://doi.org/10.1016/j.jcou.2020.101429.

[134] Z. Li, T. Yang, S. Yuan, Y. Yin, E.J. Devid, Q. Huang, D. Auerbach, A.W. Kleyn, Boudouard reaction driven by thermal plasma for efficient CO_2 conversion and energy storage, J. Energy Chem. 45 (2020) 128–134, https://doi.org/10.1016/j.jechem.2019.10.007.

[135] P. Liu, X. Liu, J. Shen, Y. Yin, T. Yang, Q. Huang, D. Auerbach, A.W. Kleiyn, CO_2 conversion by thermal plasma with carbon as reducing agent: high CO yield and energy efficiency, Plasma Sci. Technol. 21 (1) (2019), https://doi.org/10.1088/2058-6272/aadf30.

[136] Y. Wu, S.-Z. Li, Y.-L. Niu, H. Yan, D. Yang, J. Zhang, Experimental investigation of CO_2 conversion in Boudouard reaction driven by an atmospheric-pressure microwave plasma torch, J. Phys. D: Appl. Phys. (2022), https://doi.org/10.1088/1361-6463/acaeda.

[137] H. Zhang, Q. Tan, Q. Huang, K. Wang, X. Tu, X. Zhao, C. Wu, J. Yan, X. Li, Boosting the conversion of CO_2 with biochar to clean CO in an atmospheric plasmatron: a synergy of plasma chemistry and thermochemistry, ACS Sustain. Chem. Eng. 10 (23) (2022) 7712–7725, https://doi.org/10.1021/acssuschemeng.2c01778.

[138] S. Kelly, J.A. Sullivan, CO_2 decomposition in CO_2 and CO_2 /H2 spark-like plasma discharges at atmospheric pressure, ChemSusChem 12 (16) (2019) 3785–3791, https://doi.org/10.1002/cssc.201901744.

[139] O. Taylan, H. Berberoglu, Dissociation of carbon dioxide using a microhollow cathode discharge plasma reactor: effects of applied voltage, flow rate and concentration, Plasma Sources Sci. Technol. 24 (1) (2015), 015006, https://doi.org/10.1088/0963-0252/24/1/015006.

[140] C. Shin, T. Oh, T.J. Houlahan, C.H. Fann, S.J. Park, J.G. Eden, Dissociation of carbon dioxide in arrays of microchannel plasmas, J. Phys. D: Appl. Phys. 52 (11) (2019), 114001, https://doi.org/10.1088/1361-6463/aaf37a.

[141] T. Ma, H.-X. Wang, Q. Shi, S.-N. Li, S.-R. Sun, A.B. Murphy, Experimental study of CO_2 decomposition in a DC micro-slit sustained glow discharge reactor, Plasma Chem. Plasma Process. 39 (4) (2019) 825–844, https://doi.org/10.1007/s11090-019-09996-3.

[142] B. Raja, R. Sarathi, R. Vinu, Development of a swirl-induced rotating glow discharge reactor for CO_2 conversion: fluid dynamics and discharge dynamics studies, Energy Technol. 8 (12) (2020), https://doi.org/10.1002/ente.202000535.

[143] V. Lisovskiy, S. Dudin, P. Platonov, V. Yegorenkov, Plasma conversion of CO_2 in DC glow discharge with distributed gas injection and pumping, East Eur. J. Phys. (4) (2021) 152–159, https://doi.org/10.26565/2312-4334-2021-4-20.

[144] T. Ma, H.-X. Wang, J.-H. Sun, Effect of argon on CO_2 decomposition in micro-slit sustained glow discharge reactor, AIAA J. (2022) 1–10, https://doi.org/10.2514/1.J061566.

[145] S.C.L. Vervloedt, M. Budde, R. Engeln, Influence of oxygen on the ro-vibrational kinetics of a non-equilibrium discharge in CO2-O2 mixtures, Plasma Sources Sci. Technol. (2023), https://doi.org/10.1088/1361-6595/acb00d.

[146] S. Renninger, M. Lambarth, K.P. Birke, High efficiency CO2-splitting in atmospheric pressure glow discharge, J. CO_2 Util. 42 (2020), https://doi.org/10.1016/j.jcou.2020.101322.

[147] S. Renninger, J. Stein, M. Lambarth, K.P. Birke, An optimized reactor for CO_2 splitting in DC atmospheric pressure discharge, J. CO_2 Util. 58 (2022), 101919, https://doi.org/10.1016/j.jcou.2022.101919.

[148] A. Kobayashi, H. Hamanaka, Decomposition characteristics of carbon dioxide by gas tunnel-type plasma jet, Vacuum 80 (11) (2006) 1294–1298, https://doi.org/10.1016/j.vacuum.2006.01.064.

[149] J. Li, X. Zhang, J. Shen, T. Ran, P. Chen, Y. Yin, Dissociation of CO_2 by thermal plasma with contracting nozzle quenching, J. CO_2 Util. 21 (2017) 72–76, https://doi.org/10.1016/j.jcou.2017.04.003.

[150] L.M. Martini, S. Lovascio, G. Dilecce, P. Tosi, Time-resolved CO_2 dissociation in a nanosecond pulsed discharge, Plasma Chem. Plasma Process. 38 (4) (2018) 707–718, https://doi.org/10.1007/s11090-018-9893-3.

[151] C. Montesano, S. Quercetti, L.M. Martini, G. Dilecce, P. Tosi, The effect of different pulse patterns on the plasma reduction of CO_2 for a nanosecond discharge, J. CO_2 Util. 39 (2020), 101157, https://doi.org/10.1016/j.jcou.2020.101157.

[152] A. Bogaerts, E.C. Neyts, O. Guaitella, A.B. Murphy, Foundations of plasma catalysis for environmental applications, Plasma Sources Sci. Technol. 31 (5) (2022), 053002, https://doi.org/10.1088/1361-6595/ac5f8e.

[153] A. Fridman, Plasma chemistry, Cambridge university press, 2008.

[154] R.I. Azizov, A.K. Vakar, V. Zhivotov, M.F. Krotov, O. Zinov'ev, B. Potapkin, A. Rusanov, V.D. Rusanov, A.Ae Fridman, Nonequilibrium plasmochemical process of the CO_2 decomposition in supersonic UHF discharge, Doklady Akademii Nauk. Russian Academy of Sciences, 1983, pp. 94–98.

[155] A. Fridman, S. Nester, L.A. Kennedy, A. Saveliev, O. Mutaf-Yardimci, Gliding arc gas discharge, Prog. Energy Combust. Sci. 25 (2) (1999) 211–231, https://doi.org/10.1016/S0360-1285(98)00021-5.

[156] Z. Jiang, T. Xiao, V.á Kuznetsov, P.á Edwards, Turning carbon dioxide into fuel, Philos. Trans. R. Soc. A: Math., Phys. Eng. Sci. 368 (1923) (2010) 3343–3364, https://doi.org/10.1098/rsta.2010.0119.

[157] C. De Bie, J. van Dijk, A. Bogaerts, CO_2 hydrogenation in a dielectric barrier discharge plasma revealed, J. Phys. Chem. C 120 (44) (2016) 25210–25224, https://doi.org/10.1021/acs.jpcc.6b07639.

[158] S. Heijkers, R. Snoeckx, T. Kozák, T. Silva, T. Godfroid, N. Britun, R. Snyders, A. Bogaerts, CO_2 conversion in a microwave plasma reactor in the presence of N2: elucidating the role of vibrational levels, J. Phys. Chem. C 119 (23) (2015) 12815–12828, https://doi.org/10.1021/acs.jpcc.5b01466.

[159] A. Indarto, D.R. Yang, J.-W. Choi, H. Lee, H.K. Song, Gliding arc plasma processing of CO_2 conversion, J. Hazard. Mater. 146 (1) (2007) 309–315, https://doi.org/10.1016/j.jhazmat.2006.12.023.

[160] M. Kano, G. Satoh, S. Iizuka, Reforming of carbon dioxide to methane and methanol by electric impulse low-pressure discharge with hydrogen, Plasma Chem. Plasma Process. 32 (2) (2012) 177–185, https://doi.org/10.1007/s11090-011-9333-0.

[161] M. Ramakers, I. Michielsen, R. Aerts, V. Meynen, A. Bogaerts, Effect of argon or helium on the CO_2 conversion in a dielectric barrier discharge, Plasma Process. Polym. 12 (8) (2015) 755–763, https://doi.org/10.1002/ppap.201400213.

[162] A. Bogaerts, X. Tu, J.C. Whitehead, G. Centi, L. Lefferts, O. Guaitella, F. Azzolina-Jury, H.-H. Kim, A.B. Murphy, W.F. Schneider, T. Nozaki, J.C. Hicks, A. Rousseau, F. Thevenet, A. Khacef, M. Carreon, The 2020 plasma catalysis roadmap, J. Phys. D: Appl. Phys. 53 (44) (2020), https://doi.org/10.1088/1361-6463/ab9048.

[163] E. Delikonstantis, M. Scapinello, V. Singh, H. Poelman, C. Montesano, L. M. Martini, P. Tosi, G.B. Marin, K.M. Van Geem, V.V. Galvita, Exceeding equilibrium CO_2 conversion by plasma-assisted chemical looping, ACS Energy Lett. 7 (6) (2022) 1896–1902, https://doi.org/10.1021/acsenergylett.2c00632.

[164] E. Delikonstantis, M. Scapinello, G.D. Stefanidis, Process modeling and evaluation of plasma-assisted ethylene production from methane, Processes 7 (2) (2019) 68, https://doi.org/10.3390/pr7020068.

[165] J.-L. Liu, H.-W. Park, W.-J. Chung, D.-W. Park, High-efficient conversion of CO_2 in AC-pulsed tornado gliding arc plasma, Plasma Chem. Plasma Process. 36 (2) (2015) 437–449, https://doi.org/10.1007/s11090-015-9649-2.

[166] J.P. Trelles, Solar-plasma reactors for CO_2 conversion, J. Phys. D: Appl. Phys. 55 (10) (2022), 103001, https://doi.org/10.1088/1361-6463/ac3035.

[167] A.D.N. Kamkeng, M. Wang, J. Hu, W. Du, F. Qian, Transformation technologies for CO$_2$ utilisation: current status, challenges and future prospects, Chem. Eng. J. 409 (2021), 128138, https://doi.org/10.1016/j.cej.2020.128138.

[168] R. Madurai Elavarasan, R. Pugazhendhi, M. Irfan, L. Mihet-Popa, I.A. Khan, P. E. Campana, State-of-the-art sustainable approaches for deeper decarbonization in Europe – an endowment to climate neutral vision, Renew. Sustain. Energy Rev. 159 (2022), 112204, https://doi.org/10.1016/j.rser.2022.112204.

[169] D-CRBN, The fastest route to a net zero world. ⟨https://d-crbn.com/⟩. (Accessed 13 February 2023).

[170] N. applied, Improved food production with reduced emissions. ⟨https://n2applied.com/⟩. (Accessed 13 February 2023).

[171] Optanic, Scale up plasma technology for dry reforming of methane. ⟨https://www.linkedin.com/company/optanic/about/⟩. (Accessed 13 February 2023).

[172] D. Technology, We make your business sustainable. ⟨https://daphnetechnology.com⟩. (Accessed 5 December 2022).

[173] Recarbon, Carbon transformation for a healthier planet. ⟨https://www.recarboninc.com/⟩. (Accessed 13 February 2023).

Supporting information: How important is reactor design for CO₂ conversion in warm plasmas?

Rani Vertongen[1] and Annemie Bogaerts[1]

[1] Research group PLASMANT, Department of Chemistry, University of Antwerp, Universiteitsplein 1, 2610 Antwerp, Belgium.

S1. Experimental setup: 2D scheme

We present the experimental details in section 2.1 in the main paper. Here, we provide a 2D schematic of the setup to present a clear view on the connection of all components.
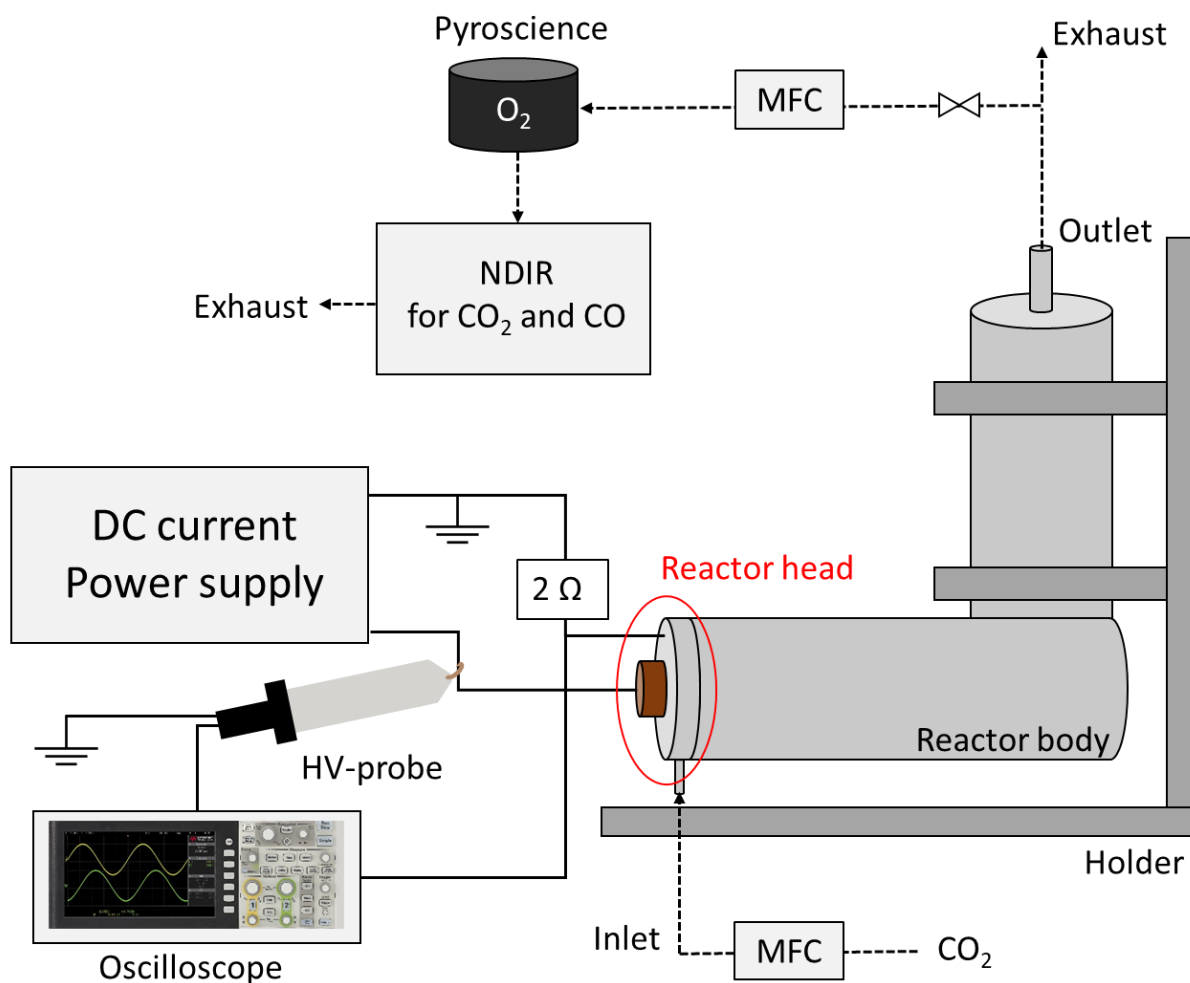

Figure SI - 1 Schematic of the experimental setup, indicating the gas circuit (dashed lines) controlled by the mass flow controller (MFC) and the electrical circuit (full lines). The reactor head is explained in more detail in Figure 2 in the main paper and previous work [1]. The reactor body has an L-shape in order to diminish the vortex flow before arriving at the diagnostics. The Faraday cage is not displayed to show each component more clearly.

S2. Overview of all electrodes and their dimensions

Table SI - 1a Overview of all GAP electrode configurations evaluated in this work. The outer shape of the electrode is displayed in dark grey, while the white space represents the gas volume. The length and diameter of the electrode are specified for each configuration, and are included in the electrode name. Unless stated otherwise, the dimensions of the electrodes are drawn to scale. The "default" reactor design that was tested by Ramakers et al. [2] is the C_{L20_d18} and A_{L16_d7} combination (indicated by the thick frame and shown in the bottom right corner).

Cathodes					
Name	C_{L10_d18}	**C_{L20_d18}**	C_{L30_d18}	C_{L20_d10}	$C_{L16\_d18\_cone}$
Length (mm)	10	20	30	20	16
Diameter (mm)	18	18	18	10	18

Anodes				
Name	$A_{L16\_d3.5}$	**A_{L16_d7}**	A_{L16_d14}	A_{L90_d7} (not on scale)
Length (mm)	16	16	16	90
Diameter (mm)	3.5	7	14	7

Table SI – 1b Overview of the GAP inserted electrode configurations evaluated in this work. The picture in the right column illustrates how the inserted anodes fit into the cathode body, with schematic indication of the arc.
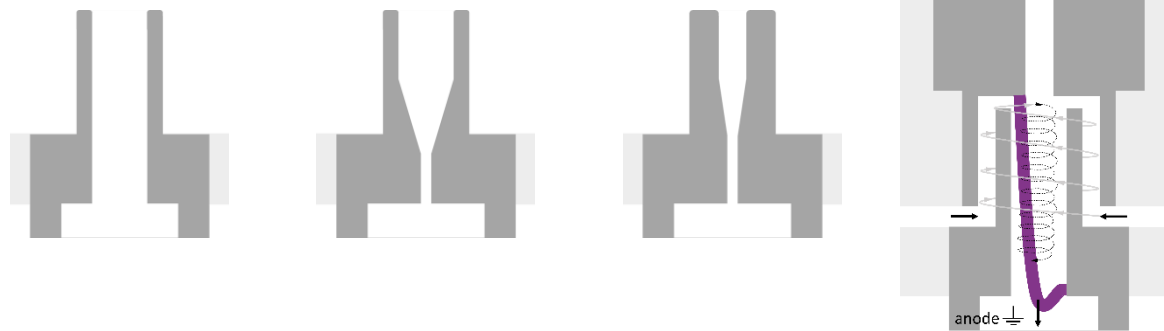
Name	$A_{insert\_L30\_d8}$	$A_{tapered\_insert\_L30\_d8}$	$A_{tapered\_insert\_L30\_d4}$	Inserted anode into cathode
Length (mm)	30	30	30	
Diameter (mm)	8	8	4	

S3. Calculation of the conversion

The conversion χ can be deduced from the stoichiometry of the reaction for pure CO_2 splitting, as indicated in Table 1.

Table 1 Reaction equation for pure CO_2 conversion, expressed in flow rates relative to the total inlet flow rate.

Reaction	$CO_2 \rightarrow$	CO	O_2
in	1	0	0
out	$1-\chi$	χ	$\chi/2$

After the reaction, we can express the measured concentration of CO_2 as the CO_2 output fraction $y_{CO_2}^{out}$:

$$y_{CO_2}^{out} = \frac{\dot{n}_{CO_2}^{out}}{\dot{n}_{tot}^{out}} = \frac{\dot{n}_{CO_2}^{out}/\dot{n}_{tot}^{in}}{\dot{n}_{tot}^{out}/\dot{n}_{tot}^{in}} = \frac{1-\chi}{(1-\chi)+\chi+\frac{\chi}{2}} = \frac{1-\chi}{1+\frac{\chi}{2}} \tag{1}$$

With $\dot{n}_{CO_2}^{out}$ and $\dot{n}_{tot}^{out}$ the CO_2 and total molar flow rate at the reactor outlet, respectively, and $\dot{n}_{tot}^{in}$ the total molar flow rate at the reactor inlet (which in the case of pure CO_2 splitting is equal to the molar flow rate at the reactor inlet $\dot{n}_{CO_2}^{in}$). For the other components, we obtain:

$$y_{CO}^{out} = \frac{\chi}{1+\frac{\chi}{2}} \tag{2}$$

$$y_{O_2}^{out} = \frac{\frac{\chi}{2}}{1+\frac{\chi}{2}} \tag{3}$$

The conversion is calculated from any of these measured fractions by simply rearranging the equations. When the output fraction of CO_2 is measured, we calculate the conversion as follows:

$$\chi = \frac{1-y_{CO_2}^{out}}{1+\frac{y_{CO_2}^{out}}{2}} \tag{4}$$

This formula inherently accounts for the gas expansion, but is only valid in pure CO_2 splitting.

S4. Effect of electrode dimensions on the measured voltage

In this section, we provide more insight in the discharge characteristics, to better understand the performance results of the various electrode designs, by studying the voltage as a function of the various design parameters. The voltage can provide insights in the length of the plasma arc, but also on the temperature of the plasma. The electrode designs change the flow pattern, which might enable better cooling of the plasma, and then the resistance of the plasma increases. At the same current, the voltage will increase according to Ohm's law. However, these trends are difficult to validate without detailed in-situ optical diagnostics, which was out of scope for this work. Therefore, the explanations in this section are meant to be indicative rather than absolute.

S4.1 Oscillographs

At a constant input current in the power supply, the voltage oscillates as a function of time, as displayed in Figure SI - 2 for three different electrode designs (i.e., the three different anode diameters). The large peaks, followed by a smaller oscillating zone, demonstrate that the arc is continuously attaching and detaching. This is in line with the properties of a gliding arc plasma and observations in previous work by our group with fast camera imaging [1].
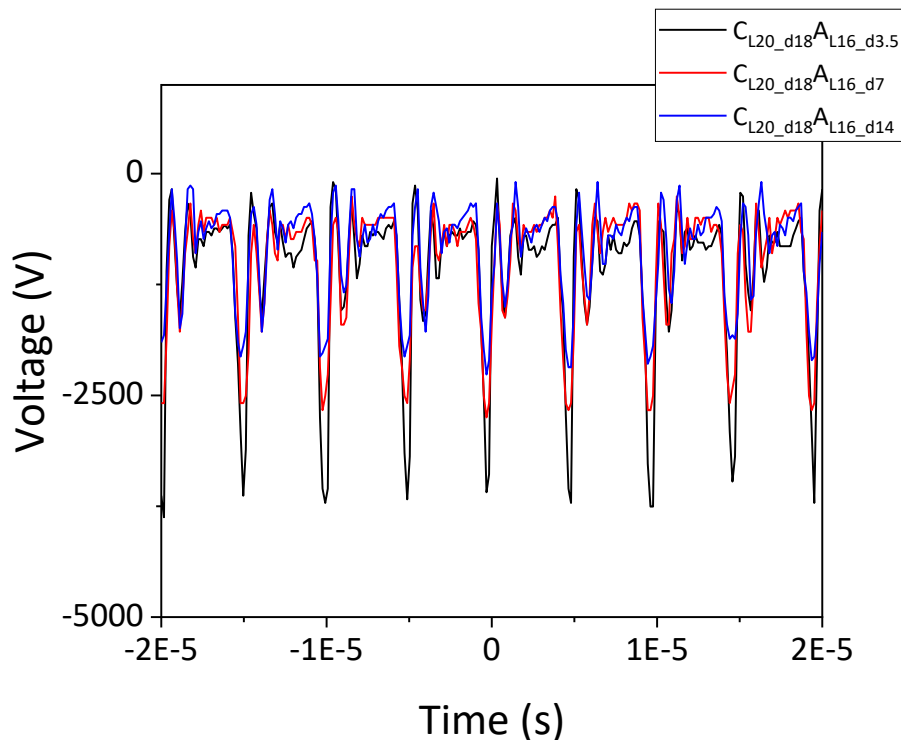

Figure SI - 2 Oscillograph, displaying the voltage as a function of time for the default cathode C_{L20_d18} and three different anodes (legend).

The smallest anode has the largest voltage peaks and seems therefore more unstable. For larger anodes, the peaks become smaller. In the next section, we will discuss this in more detail by studying the time-averaged voltage for each electrode combination.

5

S4.2 Effect of cathode length and anode diameter

The time-averaged voltage is plotted in Figure SI - 3 as a function of the anode diameter, for three different cathode lengths.
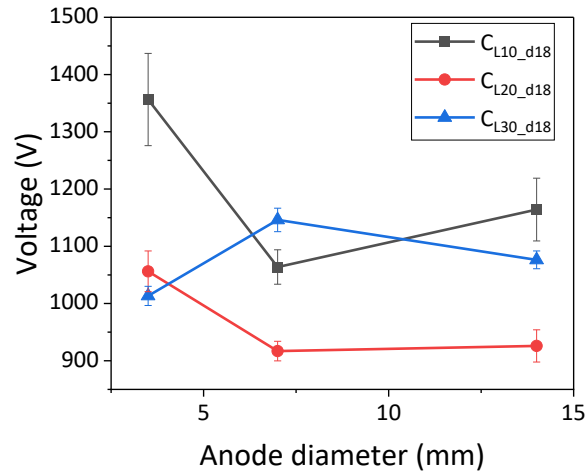

Figure SI - 3 Time-averaged voltage as a function of the anode diameter (x-axis) for three different cathode lengths (legend).

It is clear that the trend of the two shorter cathodes (C_{L10_d18} and C_{L20_d18}) are in line. The voltage remains roughly the same when decreasing the anode diameter from 14 to 7 mm, but then suddenly increases when the anode diameter drops to 3.5 mm. Probably, the arc extends more out of the reactor for a smaller anode diameter, as indeed also observed in previous work by our group for the same reactor [1]. This could explain the higher voltage, because a longer arc should correspond to a higher voltage. For the longest cathode C_{L30_d18} the trend is different: the voltage drops slightly when the anode diameter is decreased to 3.5 mm. This indicates that the plasma is contained more inside the larger cathode and thus extends less outside of the outlet when further decreasing the anode diameter.

Despite these differences in the voltage, the resulting conversion is very similar for all three cathodes, as displayed in Figure SI - 4, and the smallest outlet has the highest conversion. Indeed, independent of the cathode length, a smaller anode diameter has the most pronounced reverse vortex flow (RVF) effect, as demonstrated in previous work from our group [2, 3], which helps to improve the conversion. In addition, a smaller anode diameter also translates to a higher gas velocity at the outlet, which increases the convective cooling. This can enhance quenching once the gas leaves the reactor, similar to the effect of a nozzle after a thermal plasma, as observed by Li et al. [4]. These results indicate that for the total conversion, the anode outlet diameter, and thus the RVF effect and possible quenching effects, are more important than the time-averaged voltage.
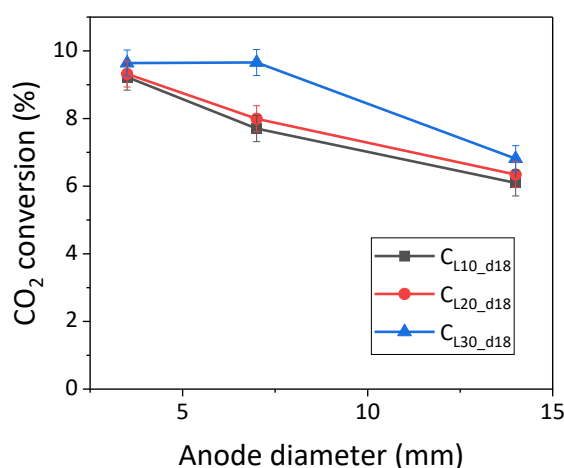
Figure SI - 4 CO_2 conversion as a function of the anode diameter (x-axis) for three different cathode lengths (legend).

S4.3 Effect of cathode and anode length

In Figure SI - 5, the time-averaged voltage is displayed as a function of the cathode length, for both the short (A_{L16_d7}) and long (A_{L90_d7}) anode.
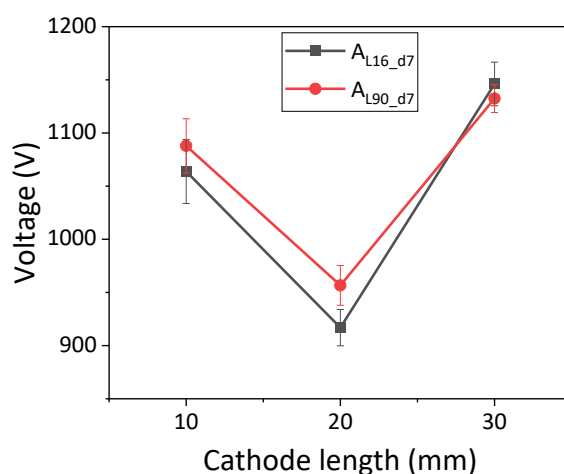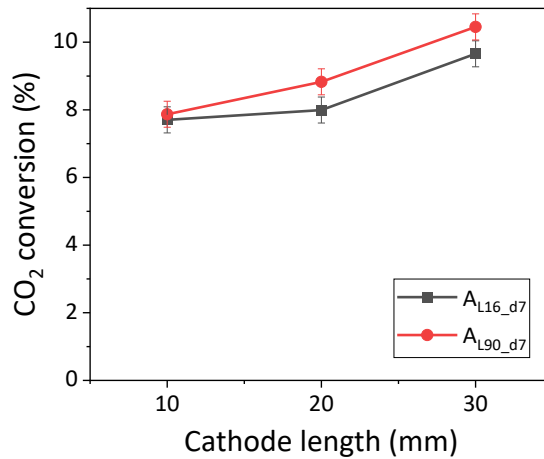

Figure SI - 5 Time-averaged voltage as a function of the cathode length (x-axis) for two different anode lengths (legend).

For both anodes, the voltage drops when decreasing the cathode length from 30 to 20 mm. Probably, the shorter cathode leads to a shorter plasma, which can explain the lower voltage. When further decreasing the cathode length to 10 mm however, the voltage increases again. Possibly, the arc extends more outside of the reactor because the smaller cathode volume cannot contain the plasma and lead to a longer afterglow.

The voltage of the longest anode is not significantly higher than for the shorter anode. There are two possible explanations for this. First, it might indicate that the plasma is not elongated significantly within the longer anode. Secondly, it is possible that the plasma is elongated in the outlet, which would increase the voltage, but that there is less cooling, which decreases the voltage again. Indeed, we observed that the configurations with the longer anode need more time to heat up before they reach a stable conversion (e.g. 7 min instead of 2 min for the shorter anodes), as discussed in the main paper. We cannot verify this just from the time-averaged voltage, but we can observe the damage from the

7

arc attachment on the anode: the shorter anodes show clear damage on the outlet, but this is not the case for the elongated anode. This supports our first explanation: probably, the arc is not elongated significantly in the longer anode.

Similar effects are observed for the conversion in Figure SI - 6. It is not significantly higher for the extended anode; hence, there is no improvement in the performance compared to the default design. Based on the time-averaged voltage, we thus hypothesize that the extended anode does not yield a longer arc, which is in line with our observation of no clear damage for this extended anode.

Figure SI - 6 CO_2 conversion as a function of the cathode length (x-axis) for two different anode lengths (legend).

S4.4 Effect of cathode and anode diameter

Figure SI - 7 displays the time-averaged voltage as a function of anode diameter for both the default cathode (C_{L20_d18}) and the smaller cathode diameter (A_{L20_d10}).
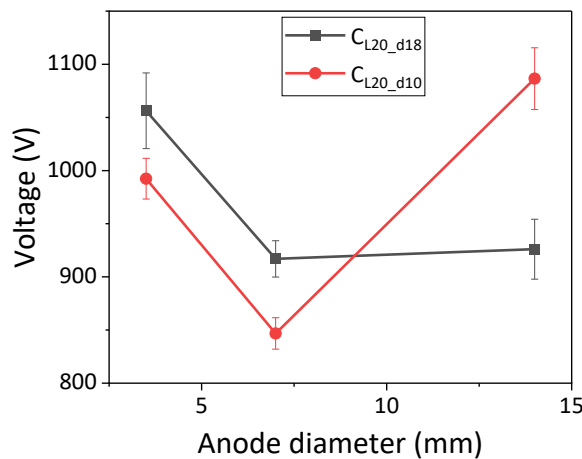

Figure SI - 7 Time-averaged voltage as a function of the anode diameter (x-axis) for two different cathode diameters (legend).

For the smaller anodes (diameter of 3.5 and 7 mm), the voltage is lower for the smaller cathode diameter. This might indicate that there is less cooling, which can indeed be expected if the distance between the hot plasma core and the walls is smaller. Then suddenly, the voltage increases for the largest anode, which might indicate that a larger anode improves the cooling. This is not the case for

the wider cathode diameter, suggesting that the properties of the discharge are indeed different depending on the cathode diameter.

If we assume that both configurations have a similar plasma length, because the cathode lengths are the same and they are combined with the same anodes, then the different voltages are a consequence only of the different cooling rates inside the cathode. Yet, the conversion is very similar for both cathodes in Figure SI - 8. This may indicate that the effects inside the cathode volume are less important than the effects at the outlet. Possibly, the conversion is largely determined by the amount of quenching at the outlet, as described in S4.2. Indeed, it has been demonstrated both experimentally [5] and my modelling [6, 7], that post-plasma quenching largely affects the overall conversion.
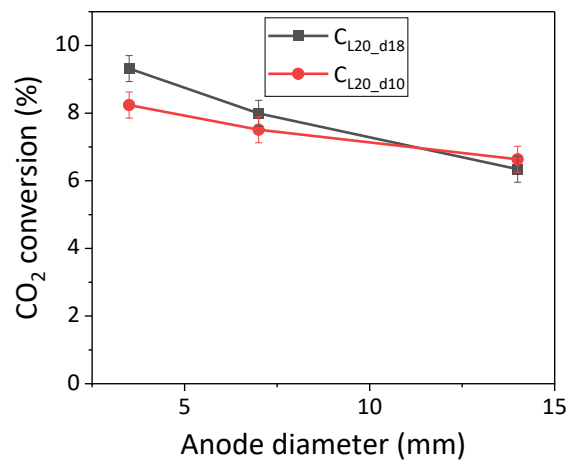

Figure SI - 8 CO_2 conversion as a function of the anode diameter (x-axis) for two different cathode diameters (legend).

S4.5 Effect of cathode shape

The time-averaged voltage is displayed in Figure SI - 9 as a function of the anode diameter for both the default cylindrical cathode (C_{L20_d18}) and for the cone-shaped cathode ($C_{L16\_d18\_cone}$).
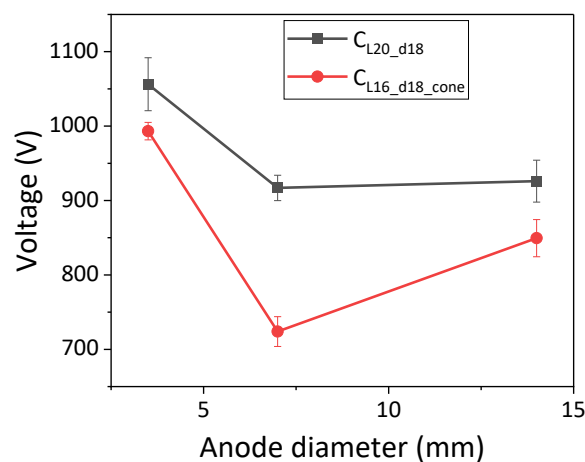

Figure SI - 9 Time-averaged voltage as a function of the anode diameter (x-axis) for two different cathode shapes (legend).

The voltage of the cone-shaped cathode is lower than that of the cylindrical cathode. Since the cone-shaped cathode is slightly shorter too, this might simply be explained by the difference in cathode length. However, the trend is very similar as for cathode with a smaller diameter (C_{L20_d10}): there is a sudden increase for the largest anode diameter, while the voltage of the cylindrical cathode remains constant. This might indicate that the cooling effects play a role again, i.e. that the cone-shaped cathode has less cooling than the cylindrical cathode.

The conversion of the cone-shaped cathode is slightly lower than that of the cylindrical cathode, as shown in Figure SI - 10. Possibly, the combined effect of the shorter cathode length and reduced cooling plays a role, explaining why the conversion is even lower than of the cathode with the smaller diameter (C_{L20_d10}) where only the cooling effects might play a role.
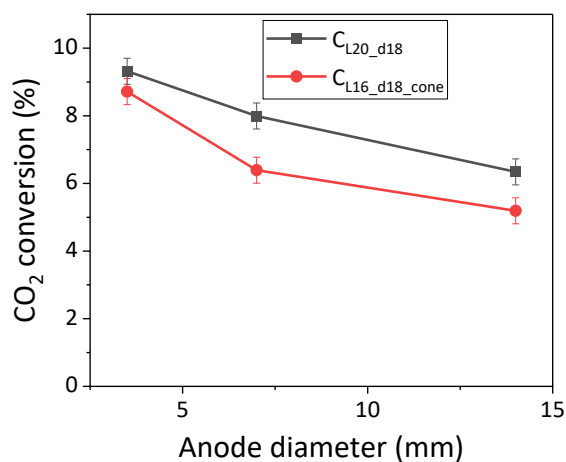

Figure SI - 10 CO_2 conversion as a function of the anode diameter (x-axis) for two different cathode shapes (legend).

S4.6 Inserted anodes

Since there is no common design parameter for the inserted anodes, we plot the time-averaged voltage as a function of the reactor volume in Figure SI - 11 for the default electrodes (C_{L20_d18}) and inserted electrodes ($C_{L16\_d18\_flat}$).
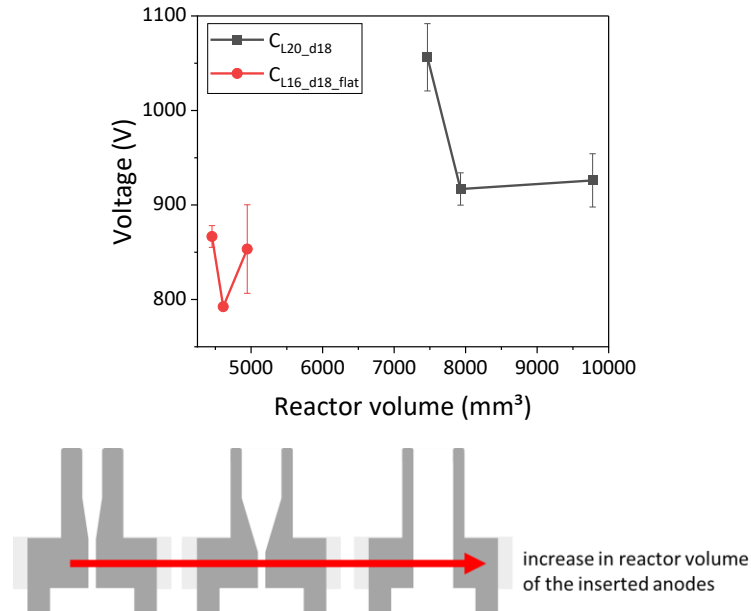

Figure SI - 11 Time-averaged voltage as a function of the reactor volume (x-axis) for the default electrode designs ($C_{L20\_d18}A_{L16\_d3.5}$, $C_{L20\_d18}A_{L16\_d7}$, $C_{L20\_d18}A_{L16\_d14}$) and the inserted electrode designs ($C_{L16\_d18\_flat}$). The increase in reactor volume for the different inserted anodes is displayed under the graph.

The voltage of the inserted anodes is lower than that of the default electrodes, which indicates that the plasma is shorter, there is less cooling or a combination of both. If the plasma does not fill the entire outlet channel, as explained in the main paper, it could form instead on the shortest distance between the cathode and the anode, as drawn in the main paper in Figure 7. In addition, the metal wall of the inserted anode inside the cathode inhibits mixing of the cold outer vortex with the warmer core, which creates a warmer plasma.

In any case, the overall stability of these electrode designs was very poor, which probably explains their low conversion, as shown in Figure SI - 12. This indicates that plasma stability is more important than plasma-gas interaction.
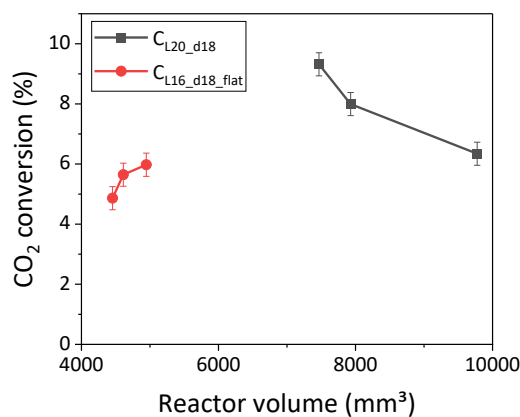

Figure SI - 12 CO_2 conversion as a function of the reactor volume (x-axis) for the default electrode designs ($C_{L20\_d18}A_{L16\_d3.5}$, $C_{L20\_d18}A_{L16\_d7}$, $C_{L20\_d18}A_{L16\_d14}$) and the inserted electrode designs ($C_{L16\_d18\_flat}$)."

11

S5. Effect of electrode shape on CO_2 conversion: higher flow rate

Figure SI - 13 summarises the performance, in terms of CO_2 conversion (a) and energy efficiency (b), at two different flow rates, i.e., 10 and 20 L_s/min, and for different cathode designs (i.e., different length, diameter or cone-shape), and the basic anode design. The power and specific energy input (SEI) are also plotted (see right y-axes). As expected, a higher flow rate of 20 L_s/min results in a lower conversion than at 10 L_s/min, for all cathode designs. In addition, the high flow rate yielded an unstable plasma for the smallest anode diameter ($A_{L16\_d3.5}$, not included here) and two of the cathodes (C_{L10_d18} and C_{L30_d18}). The inserted anodes were not included since higher flow rates led to a pressure build-up in the reactor.
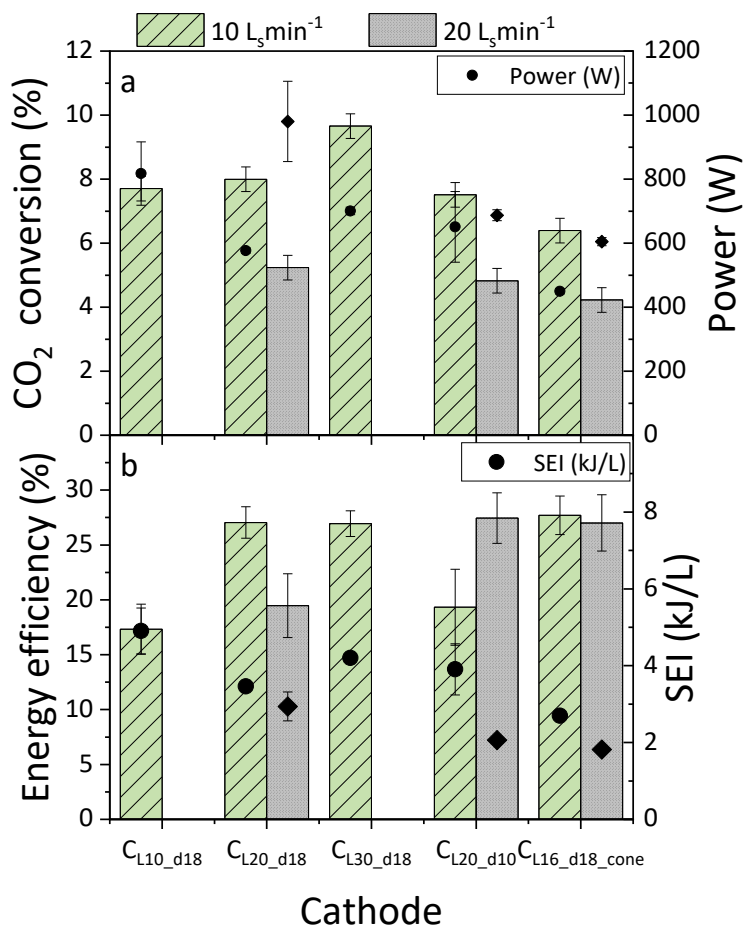

Figure SI - 13 (a) CO_2 conversion and (b) energy efficiency, presented as bars (left axis). The scatter plot represents the (a) plasma power and (b) SEI (right axis). The grouped bars represent the different cathode shapes (see x-axis), while the bar colors represent the different flow rates (see legend), all for a fixed anode A_{L16_d7}.

The higher flow rate is no guarantee for a higher energy efficiency either. For the basic cathode (C_{L20_d18}), the higher flow rate leads to a lower efficiency: the SEI is not low enough to compensate for the lower conversion. For the smaller cathode diameter (C_{L20_d10}), the higher flow rate leads to a higher energy efficiency, due to the lower SEI (indeed, similar power input but flow rate twice as high). For the cone cathode ($C_{L16\_d18\_cone}$), there is no significant difference in energy efficiency between the two flow rates. These results for the higher flow rate are included in the summarizing overview of section 4 (figure 9) in the main paper.

S6. Electrodes leading to unstable plasma and/or electromagnetic interference (EMI) issues

It is important to mention that we evaluated many more electrode shapes that were made to fit inside the same GAP reactor, with a wide range of variations in length and diameter. For a clear message in the main paper, we tried to probe the more extreme variations (e.g. the longest anode, or the cathode with the smallest possible diameter). Some electrodes were ruled out due to insights from previous work (e.g. anodes with wider diameters) [2]. In addition, some electrodes were excluded after preliminary tests that revealed unstable plasma or severe electrode damage. For the sake of transparency, and because it is useful for the reader to also learn about our "negative results", we give two examples in this section, and we explain how we dealt with the resulting electromagnetic interference (EMI) in these cases of unstable plasma.

Figure SI - 14 gives an example of two cathode configurations that gave rise to unstable plasma, i.e. the "donut" cathode and the "pin" cathode. Keep in mind that these are 2D presentations of a 3D cathode, as demonstrated on the right.
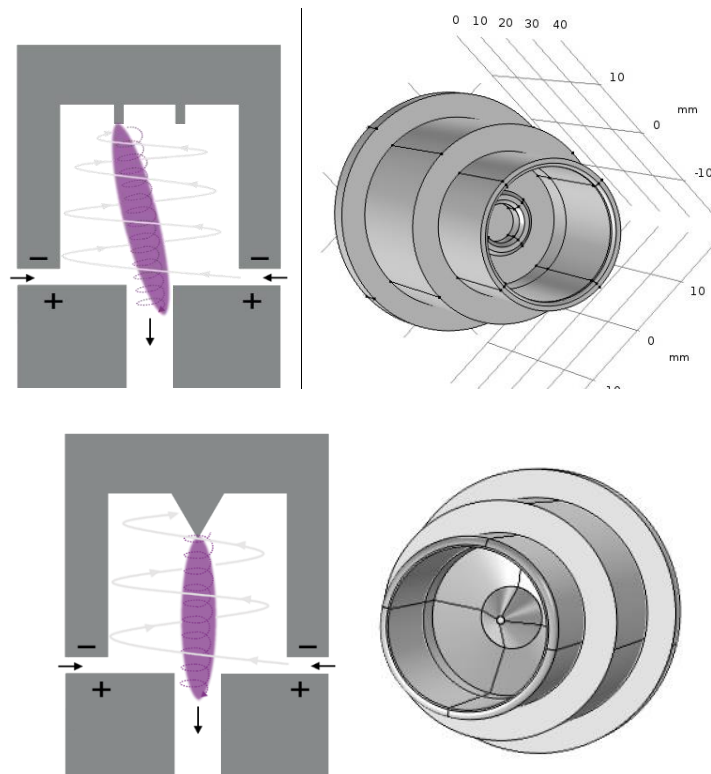

Figure SI - 14 Schematic representation in 2D (left) and 3D (right) of the donut (top) and pin (bottom) cathodes.

In both cathodes, the design idea was to play around with the location of the arc attachment. In the donut cathode, the goal was to let it rotate more in a wider volume of the cathode and thus increase the fraction of gas that is treated by the plasma. However, there was no significant difference between this cathode and the basic design. In addition, we observed significant damage in the centre of the "donut", indicating that the arc does not attach on the donut itself. Such electrode damage was even worse in the pin design. The idea here was to force an arc attachment into one point. This goal was certainly obtained, since we observed severe damage to the point. When we ran a test in the open mode (i.e. not attached to the reactor body to measure the exhaust, but open to the air to observe the plasma), the plasma was much brighter compared to the basic design, indicating that the cathode spot

is indeed much more intense. In both designs, the damage was too severe to continue the experiments, since we could not guarantee reproducibility.

These two examples, but also the inserted anodes and some operating conditions (e.g. too low power) in the other electrodes also yielded an unstable plasma. As a consequence, a lot of electromagnetic interference (EMI) was observed, with issues in nearby communication cables (e.g. USB connectors to the PC or cables from the mass flow controllers) and even an occasional shutdown of the computers in the lab. This was not an issue in the basic electrode designs, since the power supply was tailored to this type of plasma. In order to find good parameters for the flow rate and power in different electrode designs, we had to adapt the lab to account for possible EMI. Specifically, we applied the following practices for limiting EMI:

- Larger distance between the setup (power supply and reactor) and the sensitive equipment or cable.
- Routing the cables away from each other.
- Shielding the emitting device in a metal box or a Faraday cage.
- Ensuring a separate earth-ground to dissipate the EMI.
- Installing ferrite chokes as passive filters to reduce the EMI from signal or power cables.
- Reducing operating frequencies (if possible).
- Installing optocouplers in between the sensitive connections.

All of these measures are general good practices to limit the effects of interference in e.g. welding workshops, but they are also valid for plasma reactors. However, this information is usually not included in scientific literature, which makes it sometimes difficult to set up experiments for researchers who are new in the field. We hope that this short list can help plasma researchers to try and understand these issues and implement these good practices. For more information, we recommend sources on welding equipment [8] or specific literature [9].

S7. References

[1] M. Ramakers, J.A. Medrano, G. Trenchev, F. Gallucci, A. Bogaerts, Revealing the arc dynamics in a gliding arc plasmatron: a better insight to improve CO2conversion, Plasma Sources Science and Technology 26(12) (2017). https://doi.org/10.1088/1361-6595/aa9531.
[2] M. Ramakers, G. Trenchev, S. Heijkers, W. Wang, A. Bogaerts, Gliding Arc Plasmatron: Providing an Alternative Method for Carbon Dioxide Conversion, ChemSusChem 10(12) (2017) 2642-2652. https://doi.org/10.1002/cssc.201700589.
[3] G. Trenchev, S. Kolev, W. Wang, M. Ramakers, A. Bogaerts, CO2 Conversion in a Gliding Arc Plasmatron: Multidimensional Modeling for Improved Efficiency, The Journal of Physical Chemistry C 121(44) (2017) 24470-24479. https://doi.org/10.1021/acs.jpcc.7b08511.
[4] J. Li, X. Zhang, J. Shen, T. Ran, P. Chen, Y. Yin, Dissociation of CO2 by thermal plasma with contracting nozzle quenching, Journal of CO2 Utilization 21 (2017) 72-76. https://doi.org/10.1016/j.jcou.2017.04.003.
[5] A. Hecimovic, F.A. D'Isa, E. Carbone, U. Fantz, Enhancement of CO2 conversion in microwave plasmas using a nozzle in the effluent, Journal of CO2 Utilization 57 (2022) 101870. https://doi.org/10.1016/j.jcou.2021.101870.
[6] S. Van Alphen, A. Hecimovic, C.K. Kiefer, U. Fantz, R. Snyders, A. Bogaerts, Modelling post-plasma quenching nozzles for improving the performance of CO2 microwave plasmas, Chemical Engineering Journal 462 (2023) 142217. https://doi.org/https://doi.org/10.1016/j.cej.2023.142217.
[7] V. Vermeiren, A. Bogaerts, Plasma-Based CO2 Conversion: To Quench or Not to Quench?, The Journal of Physical Chemistry C 124(34) (2020) 18401-18415. https://doi.org/10.1021/acs.jpcc.0c04257.
[8] T.L.E.C. Systems, Concepts of signal noise reduction - Shielding and grounding, 2013. https://torchmate.com/news/Concepts-of-Signal-Noise-Reduction. (Accessed 31 January 2023).
[9] P. Mazurek, Chosen Aspects of the Electromagnetic Compatibility of Plasma Reactors with Gliding Arc Discharges, Applied Sciences 10(11) (2020) 3789. https://doi.org/10.3390/app10113789.